

Scaling strategies for multi-purpose floating structures physical modeling: state of art and new perspectives

Carlo Ruzzo^a, Sara Muggiasca^b, Giovanni Malara^a, Federico Taruffi^b, Marco Belloli^b, Maurizio Collu^e, Liang Li^{e,f}, Giulio Brizzi^d, Felice Arena^{a,*}

^a Natural Ocean Engineering Laboratory (NOEL), Mediterranea University, Reggio Calabria, Italy

^b Politecnico di Milano, Milano, Italy

^d CHLAMYS Srl, Trani, Italy

^e Department of Naval Architecture, Ocean and Marine Engineering, University of Strathclyde. Glasgow G4 0LZ, UK

^f Shandong Province Key Laboratory of Ocean Engineering, Ocean University of China, Qingdao 266100, China

* Corresponding Author. E-mail address: arena@unirc.it

Abstract

Multi-purpose floating platforms are emerging as a promising concept in ocean engineering applications, thanks to their capability of ensuring system integration, cost reduction and modularization. However, their increasing complexity requires the development of numerical tools, which need to be validated experimentally through adequate physical models. New challenges hence arise, since the subsystems integrated in the structure generally follow different scaling laws and may need relatively large physical models to achieve a reliable similitude between the full-scale structure and its physical model counterpart. The latter issue can be critical, because indoor tests in wave tanks and basins constrain the scale factors to the size of the available facilities. Open-sea experiments, albeit challenging because of the uncontrolled environmental conditions, could be a valid complement to the traditional indoor tests. This article proposes a review of the multi-physics scaling strategies for the subsystems usually embedded in multi-purpose floating platforms, i.e. floating support, mooring system, wind turbine, wave energy converter and aquaculture facilities, by providing a critical analysis on the relevance of the scaling factor and of the scaling strategy. The paper may also serve as a guide for practical applications involving one or several of the considered subsystems.

Keywords

- Froude scaling of floating structures
- Physical models
- Multi-purpose floating structures
- Offshore wind turbines
- Floating wave energy converters
- Floating fish net cages

Definitions

BGF – Blue Growth Farm

CFD – Computational Fluid Dynamics

DA – Dimensional analysis
DOF – Degree of freedom
FMFC – Flexible Module Flexible Connector
FOWT – Floating Offshore Wind Turbine
HIL – Hardware In the Loop
LF – Low-Frequency
MPP – Multi-Purpose Platform
ORE – Offshore Renewable Energy
OWC – Oscillating Water Column
PSD – Power Spectral Density
PTO – Power Take Off
RMFC – Rigid Module Flexible Connector
SFC – Semi-submersible Flap Combination
STAGE - Similitude Theory Applied to the Governing Equations
STC – Spar Torus Combination
TRL – Technology Readiness Level
TSR – Tip Speed Ratio
VIV – Vortex-Induced Vibrations
VLFS – Very Large Floating Structure
WEC – Wave Energy Converter

1. Introduction

Experimental modeling plays a critical role in the assessment of the dynamic behavior of floating structures. Indeed, it is preparatory to the validation and calibration of numerical models and to the assessment of the design procedures. Traditionally, experimental tests are conducted in wave tanks and basins, where a small-scale model (usually between 1:50-1:100) of the full-scale prototype is exposed to controlled environmental loads (such as wind, waves, currents), and its response is measured through sensors. In marine applications, Froude scaling laws are adopted, since they generally keep constant the ratio between the hydrodynamic and gravitational forces on the prototype and the model [1]. However, this traditional scaling approach does not account for a number of phenomena, arising in many practical cases. These limitations become particularly relevant when dealing with multi-purpose platforms (MPPs), as they generally embed in one floating platform various subsystems, each with its own dynamic laws affecting the global behavior of the structure.

MPP is an emerging concept in ocean engineering, which has the ambition of achieving multiple advantages with respect to traditional single-purpose floating platforms. The most straightforward advantage is the cost

reduction due to the sharing of floating support platform and equipment (electrical cables, mooring system, etc.) between the subsystems. In addition, subsystems may work in synergy, resulting in mutual improvements of the performances. Until now, countless MPP concepts have been proposed (e.g. [2–4]), ranging from relatively simple energy hubs (e.g. wind-wave), up to real floating cities. In the last years, a huge effort is being paid by Europe and other countries to support the research in the Blue Growth trajectory [5], resulting in several funded projects oriented to propose new multi-purpose floating platform concepts. Abhinav et al. [6] recently proposed a critical review of the state of the art from technological, environmental and socio-economic points of view. They highlighted that offshore renewable energy (ORE) and aquaculture systems are the most promising candidates for integration within MPPs, although most of the literature still focuses on coupled ORE applications only. In this regard, some worth mentioning projects are briefly mentioned. “Marina” platform project proposed three alternative concepts for wind-wave energy production, namely Spar Torus Combination (STC) [7], Semi-submersible Flap Combination (SFC) [8] and an Oscillating Water Column array with a wind turbine [9]. “H2Ocean” project [10] proposed a wind-wave energy production farm, to produce hydrogen. “MERMAID” project [11] was one of the first to explore the possibility of coupling aquaculture with ORE devices.

More recently, the ongoing “Blue Growth Farm” (BGF) [12] and “Space@Sea” [13] projects have been funded by EU for proposing more advanced MPP concepts. The former proposes an innovative box-shapes concrete platform, accommodating a 10 MW wind turbine and several oscillating water column (OWC) wave energy converters (WECs) in the forward side, as well as an automated aquaculture plant in the moonpool [14]. Indoor and outdoor (field) experimental campaigns, at different scales, will serve the purpose of validating the numerical models and demonstrating the concept at TRL 6 [15]. Instead, Space@Sea project proposes a standardized modular concept for affordable and flexible sea space utilization. Even if this concept could be used for practically any purpose, four particular applications about aquaculture, energy hub, living and maritime transport were proposed [16]. Despite the variability among the projects, the Technology Readiness Level (TRL) of MPPs is still generally very low ($TRL \leq 6$) [6]. Therefore, experimental activities are critical to complement numerical investigations and to foster the technology advancement. In this context, it is important to recognize that wind turbines, wave energy converters, and net cages for aquaculture plants cannot be simply scaled by means of Froude laws [17–21]. This is generally due to the importance of the other dimensionless ratios, such as Reynolds and others, which cannot be satisfied if a Froude scaling approach is adopted. The individual analysis of each component, although essential, is insufficient when more of them are integrated in a single multi-purpose structure, where their interaction plays a crucial role. Consequently, different scaling strategies must be adopted to ensure the appropriate observation of the coupling effects at the subsystem interfaces (e.g. resulting forces or moments) for the largest possible range of relevant load conditions. This becomes more and more challenging in the smaller-scale models, as scale effects generally become more relevant. When dealing with physical modeling in wave basins, scale factor is constrained by the available laboratory facilities. This applies to any floating structure physical model, but it may affect significantly MPPs, not only for the number of different subsystems, each requiring its own scaling strategies, but also because the size of new concepts proposed is expected to become larger and larger in the future [22,23]. Hence, complementary and/or alternative test approaches are gaining a growing attention from the research community, such as hybrid testing in wind tunnels [24,25] and open-sea experimental activities [26,27]. The former is very useful for structures embedding wind turbines, while the latter paves the way to the testing of larger-scale models, with potential cost reductions, thanks to the natural generation of the environmental loads.

The aim of this paper is to provide conceptual discussion and practical instructions on the efficient design of scale models of MPPs for indoor and open-sea testing. In particular, Section 2 introduces the reader to the general scaling principles and to the indoor and outdoor test environments, by highlighting the pro and cons of each of them. Section 3 discusses in detail the scaling strategies employed in the test of the subsystems commonly embedded in MPPs, i.e. floating hull, mooring system, wind turbines, oscillating water column

(OWC) wave energy converters and net cages for aquaculture. Each of the subsystems is discussed in a dedicated paragraph, including a flow diagram summarizing the most relevant scaling issues and strategies available today. This should accommodate the development of a variety of applications, involving either one of the mentioned subsystems (e.g. an investigation dedicated to a single component) or a multi-functional system. The role of the scale factor is critically discussed throughout the paper by providing practical criteria for the assessment of experimental setups. This simplifies the design choices of the interested reader/user, based on the critical interpretation of the information provided, in light of the specific envisaged application and the corresponding required level of detail. Finally, some conclusions are drawn, including practical guidelines for future developments in MPP testing.

2. Scaling principles

This section provides the theoretical framework and the common practices adopted in ocean engineering for designing experimental activities on physical models. The most relevant indoor and outdoor test environments are also presented.

2.1 Principles of similitude theory

Similitude theory is the branch of engineering sciences aimed to determine the conditions of similitude between systems and/or phenomena [28]. Since centuries, it has provided invaluable contribution to many engineering fields by providing the principles according to which a full-scale system (prototype) could be represented by a scaled one (model). Extended historical review of similitude theory and detailed description of its methods is out of the scope of this paper and can be found in literature (see e.g. the recent [28,29]).

In general, the similitude condition between two systems can be defined as the existence of a one-to-one correspondence between the corresponding mathematical models [30]. Formally, this can be expressed as the existence of a scale matrix Λ such that:

$$\mathbf{x}_p = \Lambda \mathbf{x}_m, \quad (1)$$

\mathbf{x}_p and \mathbf{x}_m being the vectors including all the variables of interest for the prototype and the model, respectively. The diagonal entries of the scale matrix are the scale factors λ_i of each variable x_i . Note that eq. (1) and scale factor definition could be equivalently expressed with inverse notation. Depending on the parameters of interest, different types of similitude can be defined. The most relevant ones in offshore engineering are geometric, kinematic and dynamic [31]. Geometric similitude concerns length parameters, such as boundaries of solid bodies. Kinematic similitude concerns flow patterns, i.e. the position of the particles at given times. By definition, kinematic similitude implies geometric and time ones. It can hence be equivalently expressed by using velocities (or accelerations), as governing parameters. Finally, dynamic similitude implies the former ones and concerns force parameters, i.e. the force distribution on any part of the system. To achieve the desired similitude between the prototype and the model, several alternative methods can be used. The most widely used in ocean engineering are the Dimensional Analysis (DA) and the Similitude Theory Applied to the Governing Equations (STAGE).

Dimensional analysis is the most classical approach to the planning of model experiments and is based on the well-known Buckingham Π theorem (see [32] for an extended treatment on this topic). The similitude between the two systems is achieved by the equality of a finite set of dimensionless parameters π_i . The theorem is based on the assumption that a system can be completely described by a (eventually unknown) dimensionally homogeneous relation f_1 between a finite set of N physical variables x_i . If K is the minimum number of base physical quantities q_i required to express the chosen physical variables x_i , it can be proved that f_1 can be reduced to another (eventually unknown) relation f_2 between a set of $N-K$ dimensionless parameters π_i , obtained as products between the K base quantities. In symbols:

$$f_1(x_1, x_2, \dots, x_N) = 0 \wedge \begin{bmatrix} x_1 \\ x_2 \\ \vdots \\ x_N \end{bmatrix} = \begin{bmatrix} k_{11} & \cdots & k_{1K} \\ k_{21} & \cdots & k_{2K} \\ \vdots & \ddots & \vdots \\ k_{N1} & \cdots & k_{NK} \end{bmatrix} \begin{bmatrix} q_1 \\ \vdots \\ q_K \end{bmatrix} \Leftrightarrow f_2(\pi_1, \dots, \pi_{N-K}) = 0; \pi_i = \prod_{j=1}^K q_j^{\beta_j}, \quad (2)$$

k_{ij} being opportune dimensional coefficients. The main advantage of DA approach is that it does not require the knowledge of the prototype and model governing equations. On the opposite side, however, care must be paid to the choice of the physical variables x_i , which must be necessary and sufficient to represent the target behavior, and to the definition of the dimensionless parameters π_i , which is not univocal.

STAGE approach, instead, can be used only when the governing equations of the prototype and of the model systems are known. In such a case, Eq. (1) is directly substituted to each term of the prototype governing equation. Scale factors λ_i are then obtained by enforcing the proportionality between each term of each model governing equation and the corresponding prototype term by the same factor.

2.2 Scaling laws

The practical application of the mentioned approaches in offshore engineering leads to Froude scaling laws, which are generally adopted in experimental activities involving floating structures.

As per DA principles, the number and kind of physical variables necessary and sufficient to represent the target prototype and model behaviors depend upon the specific case study. In general, dynamic similitude is required when dealing with floating structures. It follows that an ideal model should guarantee the similitude of all the forces and force distributions with respect to the prototype. Geometric and kinematic similitudes are implied by the dynamic one. Then, it is necessary to determine which forces contribute significantly to the overall dynamics, which is again application-dependent. This observation is quite relevant, since problems concerning multi-purpose floating platforms (MPPs) differ substantially from those relative to classical offshore structures. Indeed, each MPP subsystem contributes to the coupled overall dynamics with its own peculiar forces, which should be taken into account at this stage.

The classical offshore engineering approach is based on the well-known fact that inertial and gravitational forces are usually the most important when considering wave dynamics and fluid-structure interaction. The dimensionless parameter corresponding to those physical quantities is classically identified by Froude Number, which is defined as the square root of the ratio between inertial and gravitational forces, i.e.:

$$Fr \equiv \frac{v}{\sqrt{gl}}, \quad (3)$$

where v and l represent reference velocity and length values, and g the acceleration of gravity. Based on DA, Froude scaling laws apply if the model and the prototype keep the same value of Fr . As long as g and water density are kept constant too, which applies to any practical application, the scale factors for any physical quantity can be derived as summarized in Table 1.

Variable	Units	Scale factor
Length	M	λ_L
Velocity	$m s^{-1}$	$\lambda_L^{0.5}$
Acceleration	$m s^{-2}$	1
Time	S	$\lambda_L^{0.5}$
Mass	Kg	λ_L^3
Mass moment of inertia	$kg m^2$	λ_L^5

Force	N	λ_L^3
Moment	N m	λ_L^4
Angle	Rad	1
Power	W	$\lambda_L^{3.5}$
Frequency	s^{-1}	$\lambda_L^{-0.5}$

Table 1 – Froude scaling laws for the main variables of interest for floating platforms

Along with inertial and gravitational forces, there are other forces involved in the dynamics of offshore structures. Hence, there is the need to introduce other dimensionless parameters, to maintain similitude between the prototype and the model. A particularly relevant case in offshore engineering is that of viscous forces, which may be significant for slender elements such as hull cylinders, mooring lines, risers and/or sharp edges. The dimensionless parameter associated with viscous effects is classically identified by Reynolds Number, defined as the ratio between inertial and viscous forces, i.e.:

$$Re \equiv \frac{\rho v l}{\mu}, \quad (4)$$

where ρ is the fluid density and μ the dynamic viscosity. Since both are physical constants, it can be concluded that Fr and Re could be simultaneously preserved only if $\lambda_L=1$. The idea of using a different fluid with appropriate physical properties is unpractical in almost all applications. Hence, the resulting Re scale factor under Froude scaling laws is $\lambda_L^{1.5}$. The practical consequences of this scale effect for the scaled representation of MPPs will be discussed in section 3, as it leads to the adoption of STAGE approach, when necessary.

Other potentially relevant dimensionless parameters when dealing with MPPs are:

$$Ma \equiv \frac{v}{c}; Ca \equiv \frac{\rho v^2}{E}; KC \equiv \frac{vT}{L}; V^* \equiv \frac{v}{Lf}; St \equiv \frac{v}{Lf}; Sc \equiv \frac{2\pi h m_L}{\rho L^2}; Eu \equiv \frac{\rho v}{\Delta p}. \quad (5)$$

Mach number Ma is defined as the ratio between the local flow velocity v and the sound speed c in the medium. It physically represents the square root of the ratio between inertia and compressibility forces and is used when flow compressibility effects are relevant. In the context of MPPs, Cauchy number Ca is generally used to deal with structural flexibility, E being the Young modulus of the material. It is worth mentioning that Ca replace Ma in fluid dynamics to describe fluid compressibility by using the bulk modulus of elasticity of the fluid K instead of E in the definition. Keulegan-Carpenter number KC is the ratio between inertia and drag forces in an oscillatory flow of period T and is widely used in ocean engineering to take into account viscous effects, L being the reference length of the structure (e.g. a cylinder diameter). Reduced velocity (or conversely reduced frequency) V^* is important for assessing the impact of structure dynamics on aerodynamics and vortex shedding phenomena. It is defined as the ratio between the time needed by the flow to move through the reference length L of the structure and its natural period $T = 1/f$. Strohal number St physically represents the ratio of inertial forces due to local acceleration of the flow and to the convective acceleration and is defined analogously. It becomes of particular interest when the effects of vortex-induced vibrations (VIV) are significant [33], e.g. when dealing with taut mooring lines. Scruton number Sc is important in vibration phenomena and is defined as the product between the non-dimensional structural damping h and the mass ratio, m_L being the unit mass of the structural element and ρ the fluid density. Finally, Euler Number Eu is the ratio between inertia and pressure forces, Δp being the pressure force per unit area.

2.3 Indoor and outdoor laboratory environments

2.3.1 Indoor facilities

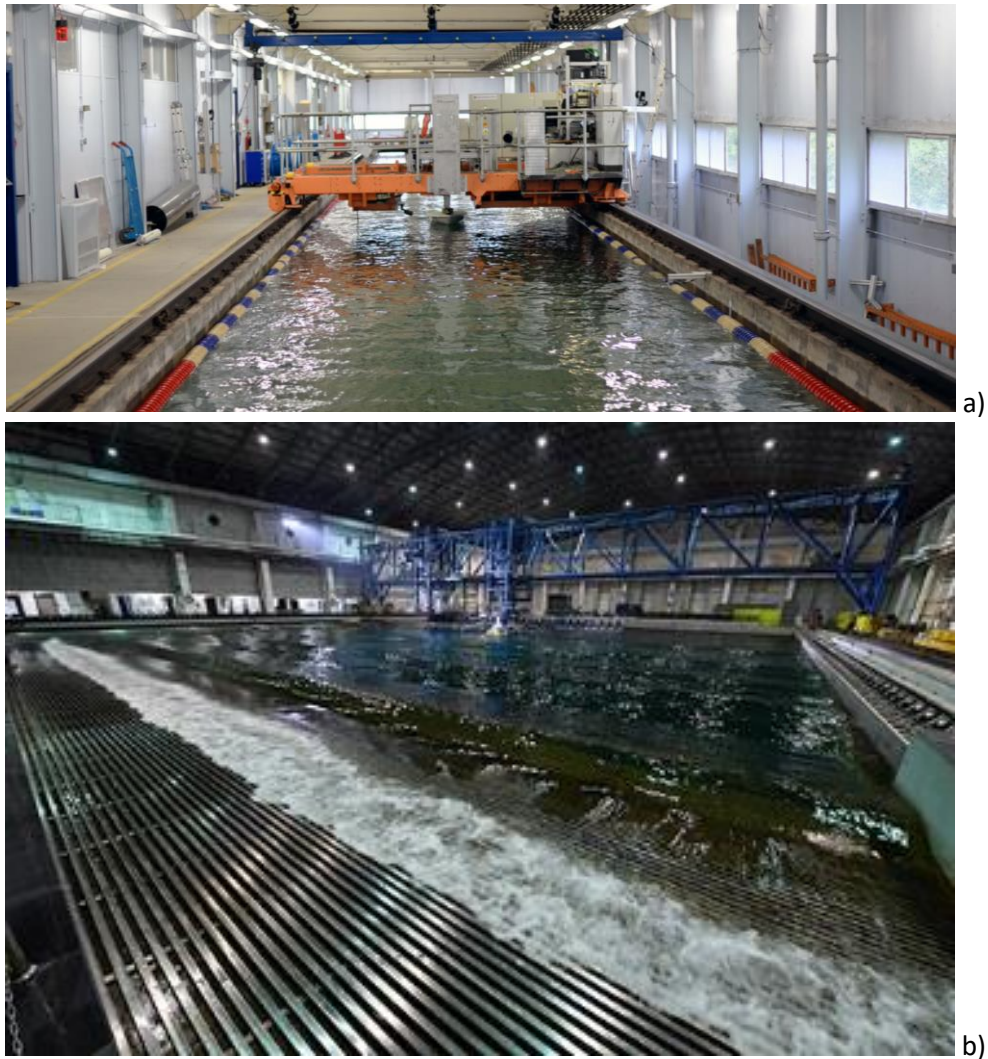


Fig. 1 – Representative examples of wave tank (a) and wave basin (b), i.e. Kelvin Hydrodynamic Laboratory [34] and State Key Laboratory of Ocean Engineering, Deepwater Offshore Basin [35], respectively.

Indoor facilities are frequently used to reproduce in scale the environmental conditions (waves, but for some also currents and, more recently, winds) that a MPP will be subject to, and to measure the response of the platform to the- scaled environmental loads. A typical towing tank has one dimension much larger than the other, it is filled with fresh water, and it is equipped with a towing carriage (Fig. 1a). This equipment is used to tow the model at a prescribed velocity to experimentally measure its resistance [36]. This kind of tests is frequently needed for ships and other floating bodies with a dimension significantly larger than the other two, and a port/starboard (left/right) symmetry. In the context of MPPs, it can be used also for individual structure sub-systems, such as fish cages, to assess the drag coefficients under current conditions. Often, a wave generation system is located at one end, and a wave-absorbing system is installed at the other, to minimise the undesired wave reflection. Due to their limitations in size, such tanks can usually generate only mono-directional waves. Historically, towing tanks were developed for the design and analysis of ships, so following the substantial expansion of O&G offshore structures in the 1950s-60s, new testing facilities were required to test stationary systems such as oil rigs, requiring a much larger area and the ability to generate complex, multidirectional sea states: wave basins (also called ocean basins). A typical wave basin is a water pool with similar sizes in length and width and a water depth generally larger than a towing tank (Fig. 1b). Some wave basins have a variable depth floor and/or a central pit with a larger depth. Unlike a 2D tank, a wave basin is usually equipped with wave generating systems over two perpendicular sides, enabling it to generate multi-directional waves. On the other sides, wave-absorbing systems are equipped to reduce wave

reflection as much as possible. In addition, current and wind generation devices may be installed as appropriate. The larger floor area also allow to model in scale the station-keeping systems (as a whole or in part, using hybrid techniques [37,38]). The employment of wave basin in the model test of MPP has been reported e.g. in [39]. Nevertheless, there are still several limitations with the use of wave basin. First, wave reflection is very difficult to eliminate completely, limiting the useful length of the experiment and/or introducing some phenomena not representative of the full real-scale situation. This is particularly relevant if low-frequency (LF) motions of the model are to be investigated, which may be of great interest for MPPs. Often, wave basins cannot model a sloped seabed, substantially limiting the possibility to test platforms in near-shore, shallow water environments. Limitations apply also to maximum and minimum water depth and wave size, which may have significant impact on the choice of the scale-factor, particularly in case of relatively large floating structures, such as many MPP concepts. A similar issue may finally apply due to the high- and low-frequency cut-offs of the wave makers, which may limit the ability to model wide-banded wave spectra depending on the scale factor. For further info about wave tanks and wave basins, the reader may e.g. refer to [40].

It is also worth mentioning that some variability in the nomenclature of wave generation facilities is found in literature and in common use, with respect to that proposed in this paper. For example “wave tank” could represent the here defined “wave basin” [41]. Finally, “wave flume” could be used for indicating 2D facilities [42].

2.3.2 Wind tunnels

A wind tunnel (Fig. 2) is a tool designed to carry out experiments for solving aerodynamic problems involving the fluid-structure interaction. Despite the possibly different layouts, all wind tunnels have four basic parts: 1) a contoured duct to control the passage of the working fluid through the test section where the model is mounted; 2) a drive system to move the working fluid through the duct; 3) a physical model of the test object; 4) an instrumentation equipment (e.g. to measure wind force, pressure). The wind tunnel facility is able to generate a controlled flow condition. Moreover, wind tunnels make it possible to use reduced-scale models, since tests on prototypes may be often too expensive or not feasible. Boundary layer wind tunnels are capable of simulating natural winds. So far, wind tunnel activities on floating structures have been mostly focused on traditional FOWTs [25,43–45], however the same logic can ideally apply to MPPs as well. Testing a wind turbine in a wind tunnel allows a good reproduction of the wind loads acting on the wind turbine rotor, assured by a controlled and high-quality flow, and a correct representation of the wind profile. Even if the dimension of the model are far from the prototype, properly scaling the wind turbine components permits to overcome scale effects. In particular, wind turbine model blades feature low-thickness profiles designed on purpose to cope with the Reynolds number difference. The remaining Reynolds scaling effect can be considered acceptable if compared with e.g. wave basins with fans. FOWTs are tested in wind tunnel following a hybrid approach. The hybrid/Hardware-In-the-Loop (HIL) technique developed at Politecnico di Milano founds on three steps: 1) the turbine subsystem is physically reproduced; 2) the floating subsystem is numerically modelled and executed in real-time, by reproducing the rigid-body dynamics, the hydrodynamic loads due to incident waves/currents and mooring lines response; 3) the two subsystems are coupled by means of a real-time measurements and actuation chain [25]. This approach could be adapted for wind tunnel tests on MPPs, when an accurate reproduction of the aerodynamic loads of the wind turbine and/or its effect on the overall MPP dynamics is required. However, the effectiveness of the hybrid approach strongly depends on the numerical capability of accurately represent the hydrodynamic behavior of the MPP, which may be questionable due to its own complexity.



Fig. 2 – Representative example of a wind tunnel, i.e. GVPM facility [46], with a wind turbine model tested by means of HIL technique.

2.3.3 Field laboratories

Based on the mentioned limitations of the indoor test facilities, outdoor environment can represent a potential alternative/complement for experimental campaigns on floating offshore structures. The following ideal classification could be proposed for outdoor activities: 1) prototypal campaigns on close-to-full-scale floating platforms (see e.g. [47,48]); 2) intermediate-scale experiments performed at sea [15,27]. Actually, the distinction between these two classes is rather arbitrary (see e.g. [49] for a hybrid case). However, the following descriptions could be proposed. Prototypal activities are usually carried out by government agencies/bodies and/or international companies to demonstrate mature concepts (TRL 7-9), with scale factors $\lambda_L \leq 10$. In most cases, they precede commercial development. Thus, the collected data are secreted and cannot be found in the open literature. These activities are generally carried out in sheltered coastal areas, or directly in offshore test sites. Due to the maturity of the concepts tested, such activities are generally devoted to the demonstration of the concept in real operational and extreme conditions [47] and to the calibration of existing numerical models. Thus, the latter are usually implemented ad-hoc, based on the specific physical model used for the test (model-of-the-model approach). Instead, at-sea intermediate-scale activities are oriented to research and development of new concepts (TRL 5-7), and are conceptually similar to indoor activities, but with scale factors $\lambda_L \leq 30$ and outdoor environment. In the last years, a growing interest for these activities has been recorded from research centers and offshore companies, as the growth in size and complexity of the proposed floating structure concepts, especially in the case of MPPs, requires further intermediate steps between small-scale indoor experiments (TRL 3-5) and prototypal activities. Based on these considerations, a detailed comparison between traditional indoor experiments and intermediate-scale outdoor activities is here presented, to support decision-making in the planning of the experiments (see also [15] for a practical application on a MPP concept)

Along with the reduction of scale effects, outdoor activities have several advantages. The natural generation of the environmental loads reduces costs significantly, and allows to perform experiments on a much longer time scale. This is quite useful, especially for probabilistic analyses [50] and investigation of low-frequency dynamic effects. On the other hand, the main challenges of such activities relate to the site-dependent uncontrolled testing environment. It is impossible to perform regular waves or white noise conditions tests

and it is quite challenging to conduct free-decay tests. Instead, the model is continuously exposed to irregular waves, winds and currents. Consequently, different analysis techniques are required for interpreting the experimental data. Direct analysis of time series, related statistical quantities and power spectral density (PSD) functions are widely used for numerical/experimental comparison [47,48]. Ruzzo et al. proposed a more detailed ad-hoc framework in a series of paper [27,51–53], combining spectral analyses and output-only techniques for the complete identification of the model dynamics. It is worth mentioning that the corresponding damping estimations proved to be more accurate than those obtained in small-scale indoor tests, particularly in case of nonlinear structure dynamics. In this context, it is crucial to measure the incoming waves at a certain distance from the structure, to estimate the motion Response Amplitude Operators (RAOs) from input/output spectra. Such a distance must be large enough to make the diffraction and radiation effects associated with the structure dynamics negligible at the measuring location, and small enough to ensure that the recorded sea state is indeed the undisturbed incident sea state exciting the model.

When dealing with intermediate-scale outdoor activities, the site selection is crucial to achieve reasonable operational and ultimate conditions for the model. With reference to experiments on waves and fixed structures, Boccotti [54] observed that most of marine sites are not suitable for experimental activities, since local waves of opportunely small size are not wind-generated, i.e. their spectra are not scale models of any meaningful full-scale conditions. Based on this observation, he identified the location of the Natural Ocean Engineering Laboratory (NOEL) in Reggio Calabria (Italy) [55,56] (Fig. 3), where the peculiar geographical and met-ocean conditions lead to the natural generation of small wind-generated waves, with significant wave height $H_s = 0.20\text{-}0.80$ m, peak period $T_p = 2.0\text{-}3.6$ s and JONSWAP-like spectra. These waves are generated by a wind blowing on a 10Km fetch. Lakes were also indicated as alternative promising outdoor environments for intermediate or small-scale outdoor activities. When dealing with floating structures, also additional wave conditions, not representative of any scaled sea states, may be useful for the experimental activities. This is because swells and mixed sea states may provide significant energy content in a wider frequency range, facilitating frequency domain identification (RAOs) of the model. Site selection should also be based on the extreme local environmental loads, governing the safety requirements of the model, and on bathymetry, governing the mooring system design. It is worth noting that all the above considerations are applicable also to the case of prototypal activities. However, in such cases, the site selection does not depend much on the scaling purposes, due to the greater size of the model. Target wind, wave and current characteristics, indeed, are closer to the full-scale case. In addition, the interest in exact scaled representation of the concept features is reduced in these cases, in favor of a more practical model-of-the-model approach, as mentioned above. Based on all these considerations, many temporary or permanent test sites and field laboratories are established all over the world for outdoor testing purposes.



Fig. 3 – Representative example of a field ocean laboratory, i.e. NOEL facility [55], with a model of a fixed breakwater embodying a wave energy converter.

3. Multi-purpose floating offshore structures scaling strategies

The aim of this Section is to provide a critical review of MPP scaling procedures by a detailed discussion of the challenges related to their common subsystems and the potential strategies to overcome them. Each paragraph considers a specific subsystem.

3.1 Hull hydrodynamic forces

Hydrodynamic forces on floating structures can be induced by waves and/or currents. It is common practice in offshore engineering (see e.g. [54,57]) to distinguish at least three cases in which wave diffraction (potential theory), inertial (Froude-Krylov) or viscous forces (Morison's equation) are dominant, respectively. The distinction is usually based on the values of rather arbitrarily defined dimensionless ratios, depending on structure size and wave characteristics (height and wavelength). Taking e.g. Faltinsen's indications [57] as a reference, the hydrodynamic force of a wave of given height H and length L on a circular cylinder of diameter D is diffraction-dominated for $D > 0.2L$, while it is viscous-dominated for $D < 0.1H$, as long as the wave does not break. When viscous forces play a secondary role on the overall hull dynamics, Froude scaling laws apply, as discussed in Section 2.2. Instead, their validity is questioned if viscous forces from waves and/or currents become not negligible, i.e. when the hull comprises relatively slender elements, as a non-negligible dependence on Reynolds number Re arises. The importance of preserving the model-prototype similitude of the viscous forces could be significant in the case of floating MPPs. This is the case of hulls comprising slender cylinders (see e.g. STC and SFC MPPs [58]). Although absolute drag forces are often significantly smaller than the inertial ones in the vast majority of practical cases, they may represent the primary source of hydrodynamic damping, whose realistic assessment is among the main challenges of experimental activities devoted to numerical model calibration. In addition, their relative importance increases when dealing with extreme wave loads, which are of absolute interest for the ultimate design conditions of any offshore structure. Although some approaches have been already proposed in literature to deal with Re distortion at small scale, such as the use of turbulence stimulators [31], the problem is still open. In the following, an alternative approach, based on the definition of a limit scale factor, will be described.

The well-known Morison's equation [59,60] is widely used to describe overall hydrodynamic forces on slender cylinders. In the context of floating offshore structures, it can be written as:

$$\mathbf{f}(t) = (1 + C_a) \rho \pi R^2 \mathbf{a}(t) - C_a \rho \pi R^2 \ddot{\mathbf{x}}(t) - C_d \rho \pi R |\mathbf{v}(t) - \dot{\mathbf{x}}(t)| [\mathbf{v}(t) - \dot{\mathbf{x}}(t)], \quad (6)$$

where \mathbf{f} is the 3-DOF time-dependent hydrodynamic force vector per unit length and normal to the cylinder, C_a and C_d are the hydrodynamic transverse added mass and drag coefficients, respectively, ρ is the water density, R is the cylinder radius, \mathbf{a} , $\ddot{\mathbf{x}}$ are the time-dependent water particle and structure accelerations and \mathbf{v} and $\dot{\mathbf{x}}$ are velocity vectors normal to the cylinder, respectively. The dependence on Re is given by the hydrodynamic coefficients C_a and C_d . Sarpkaya and Isaacson [61] proposed to determine them as functions of Reynolds and Keulegan-Carpenter numbers, through the experimental curves shown in Fig. 4. Their results were substantially confirmed by recent at-sea measurements on horizontal and vertical fixed cylinders [62,63], are commonly referred to in scientific literature (see e.g. [31,64]) and are consistent with recommended procedures for the design of offshore structures [65]. They will be hence taken as a reliable reference in the following, with reference to cylindrical slender bodies, which are the most relevant case for realistic MPP geometries. Similar results can be found for the drag coefficients of other hull shapes in literature [66], which allows extending the treatment to the specific case of interest, if needed. The cases of mooring lines and fish cages will be treated instead in Sections 3.2 and 3.5, respectively.

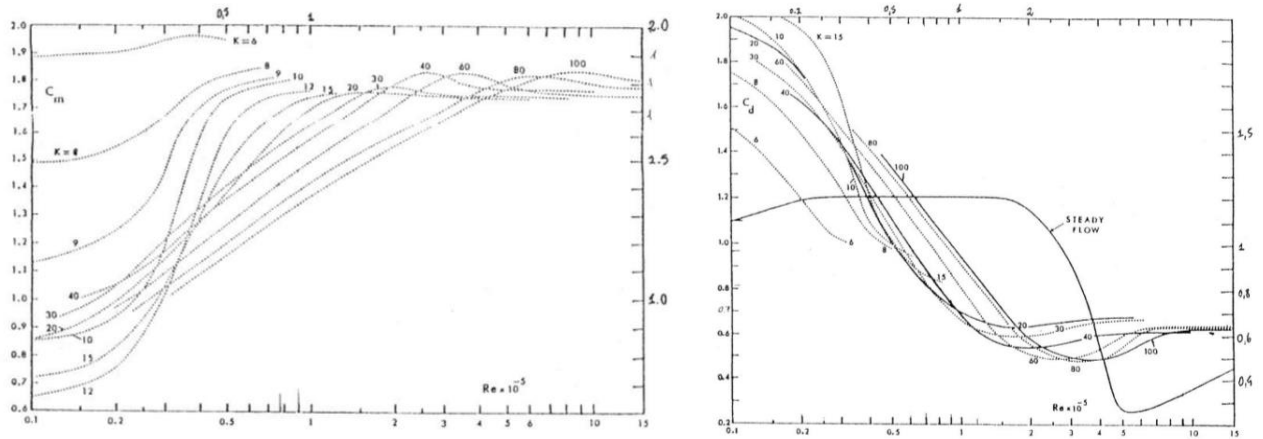


Fig. 4 – Inertia ($C_{in} = 1+C_d$) and drag (C_d) hydrodynamic coefficients for slender cylinders [61].

KC is conserved through Froude scaling. Therefore the scale effect is given by the alteration of Re only. Based on the results shown in Fig. 4, the variation of the hydrodynamic coefficients is generally assumed negligible in literature [31,67] as long as the following practical criterion is met:

$$Re > 10^5. \quad (7)$$

Criterion (7), however, has two main drawbacks:

- 1) It is strongly wave-dependent, since Re depends on both wave height and period. Furthermore, for floating structures it depends also on the instantaneous structure velocity.
- 2) Actually, hydrodynamic coefficients variations are not always negligible within the limit given by condition (7). In particular, based on the results of Fig. 4 itself, variations up to about 25% and 50 % can be observed in the inertia and drag coefficient, respectively, depending on KC . This scale effect could be particularly relevant when a good precision is required, e.g. for the calibration of damping values of slender offshore floating structures.

Following these observations, it would be opportune to reformulate criterion (7), so as to involve a ratio between Re and KC . Boccotti [1] proposed:

$$\frac{Re}{KC} = \frac{\rho D^2}{\mu T} > 10^4. \quad (8)$$

It is interesting to note that criterion (8) depends only on wave period and structure size. Also, it is more restrictive than (7), leading to maximum variations of both coefficients up to about 5%. This criterion is usually respected at full-scale for any practical case, hence it can be used straightforwardly to determine a limit scale factor $\lambda_{L,max}$ for a physical model under Froude scaling laws:

$$\lambda_L < \lambda_{L,max} = \left(\frac{\rho D_p^2}{10^4 \mu T_p} \right)^{\frac{1}{1.5}}. \quad (9)$$

It is worth noting that the maximum λ_L admissible decreases with decreasing diameter and increasing period. Consequently, small-scale models can lead to significant distortions of damping predictions, especially in extreme wave conditions and in case of low-frequency (LF) motions of offshore structures. To support these observations, it is useful to consider the reference case of OC3-Hywind spar FOWT [68] having a surface-piercing diameter of 6.5 m, which has been widely investigated in the recent scientific literature. All the up-to-date indoor experimental activities referred to this concept have been performed with scale factors

between $\lambda_L = 50-128$ [69–72]. According to the practical criterion (9), $\lambda_L = 50$ may be acceptable only for $T \leq 12s$, while $\lambda_L = 128$ is not acceptable at all. This questions the accuracy of the similarity of these models, not only in waves, but especially around the natural periods (e.g. damping estimation from free decay tests), i.e. $\sim 32-36s$ for vertical motions and $>100s$ for horizontal motions at full-scale. This could also explain the significant uncertainties of damping estimations, observed among different experiments and far greater for horizontal motions. In this context, low-cost intermediate-scale open-sea experimental activities [27] could represent an attractive alternative, as they enable better hydrodynamic similitude in the range of periods of interest. Similar considerations may apply to any floating structure, including MPPs, as long as it comprises relatively slender cylinders in its hull. Thus, the proposed strategy can be used as fast and practical means of evaluation of the scale effect for such structures, with reference to wave-structure interaction and free decay tests. Criterion (7) and direct application of the abacuses (Fig. 4) are instead suggested for the assessment of similitude accuracy for steady current loads.

Another aspect of the hydrodynamic scaling assessment of MPPs may be related to the representation of structure elasticity. It plays a non-negligible role in the overall coupled dynamics of Very Large Floating Structures (VLFS), generally defined as floating structures whose longer size is greater than 10^3 m [23]. Such structures may be regarded as a frontier for MPP concepts, since they would provide large new areas available for any activity, up to the limit of floating cities [22,23,73]. The scaling of a VLFS is very challenging, mainly because of two issues: 1) the large dimensions of the platform; 2) the scaling of the bending stiffness. A detailed treatment of this subject may be found in Ref. [74]. Here, the main issues and some possible solutions are highlighted, also in view of up-to-date research developments. The size of the VLFS represents a primary problem in scaling, particularly for indoor laboratories. Indeed, the space availability is limited. Thus, a case-dependent minimum scale factor $\lambda_{L,min}$ must be applied, which may induce significant scale effects. Wave generation could also become challenging, due to the small wave size required for high λ_L . It could be concluded that further development of model test activities on VLFS is likely to take place in outdoor environment, where smaller λ_L can be applied. With respect to the bending stiffness issue, it is useful to refer to two limit cases: 1) fully-elastic floating platform, i.e. made up of a large single body or a rigidly-jointed set of individual modules; 2) rigid-module flexible-connector (RMFC) case, i.e. a set of almost rigid modules, connected by flexible joints. In both cases, coupled hydro-elastic dynamic behavior must be represented in the model, either by taking into account module or connector flexibility, and assessment of maximum deformations and internal solicitations are of utmost importance for the study of the concept. Clearly, hybrid concepts may be of interest as well, where both the flexibility of the modules and the connectors should be represented (FMFC) [75]. As a rule of thumb, for relatively slender VLFS, the following practical criterion can be considered [76]:

$$L_C = 2\pi \left(\frac{EI}{k_C} \right)^{\frac{1}{4}}, \quad (10)$$

where EI is the equivalent bending stiffness of the structure, regarded as a beam and k_C is the spring constant of hydrostatic restoring force. The characteristic length L_C represents the locally deflected region by a static concentrated load and can be regarded as an upper limit for a rigid module, after which module flexibility cannot be neglected.

Fully-elastic structures ($L > L_C$) must be scaled taking into account the structure flexibility. Numerically, such structures are usually represented by means of simplified elastic isotropic beam [77,78] or plate [79,80] models. In both cases, assuming that the external geometry is scaled by means of Froude laws, the key parameter for the representation of the elasticity is the equivalent bending stiffness EI , with scaling factor λ_L^5 . This could be challenging to achieve while keeping geometry and mass requirements. For this purpose, opportune cross section shapes and materials should be used. Ding et al. [78], e.g., built the physical model

of a semi-submersible VLFS in glass-fiber-reinforced plastic, with wood frames. This approach becomes more and more challenging as the size of the VLFS and λ_L increase, and when a real three-dimensional internal geometry of the VLFS is to be represented. RMFC approach [81,82], instead, can be applied for structure whose modules are relatively small ($L < L_c$) and rigid, with respect to the flexible connectors. This feature appears to be growing in importance in recent research, as it reduces VLFS internal loads and facilitates modularization, with significant economical and architectural benefits [16,83]. Experiments of such modular structures are facilitated, since it is sufficient to scale the stiffness of the connectors according to Froude laws [84,85]. Finally, model tests can be realized for limited numbers of modules, thus also facilitating activities in indoor laboratories, thanks to the reduced overall size of the structure to be tested. In this regard, critical components, such as the windward modules, those hosting wave energy converters, and others, should be favored for physical representation in the tests. Finally, the variability of the dynamic response with the number and/or layout of the modules is of great interest, due to the scale-extendibility of the structures.

In conclusion, the scaling of the hull dynamic behavior is based on Froude laws, however special cases may apply if relatively small or very large floating bodies are concerned, which may be the case of MPPs. In such cases, the choice of the scale factor (highly dependent on the testing environment) plays a crucial role for the scaling accuracy. A detailed discussion on this topic has been carried out in this section, and a simplified workflow for practical applications may be found in Fig. 5.

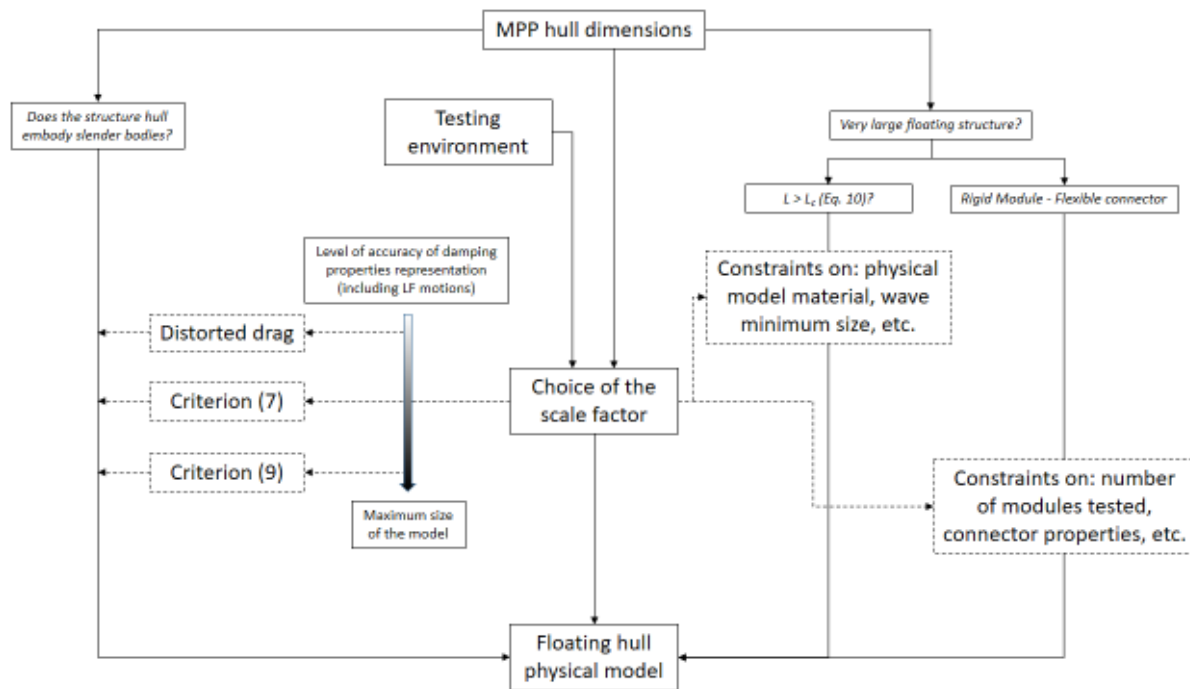


Fig. 5 – Proposed schematic workflow for the design of scaled floating hull for MPPs.

3.2 Mooring system

Mooring system represents a crucial component of any floating structure. At least, it provides station-keeping, i.e. opportune stiffness with respect to horizontal motions. In certain cases, it could also play an active role, e.g. in wave energy conversion [86] or load reduction [87]. A complete classification of mooring system categories and related mathematical models is out of the scope of the present work and can be found in up-to-date studies (see e.g. [88,89]). In general, however, two limit cases can be identified, at least for passive systems, whose schematic behavior is shown in Fig. 6 and briefly described below:

1. Catenary mooring systems, which achieve restoring forces only through their own weight. Mooring lines (quasi-slack) are suspended from the fairlead and a significant portion lay on the seabed. When the floating structure moves, all the mooring lines alter their suspended length and shape, with respect to the equilibrium position, thus providing a global restoring force to the structure. As long as the seabed is horizontal and a portion of the line lays on it, they transmit only horizontal forces to the anchor.
2. Taut leg mooring system, which achieve restoring forces only through their axial stiffness. In this case, the mooring lines (tendons or tethers) are pre-tensioned by an excess of buoyancy of the floating structure. As long as they keep taut, they provide a certain restoring force, dependent on the elongation associated with the floating structure movement.

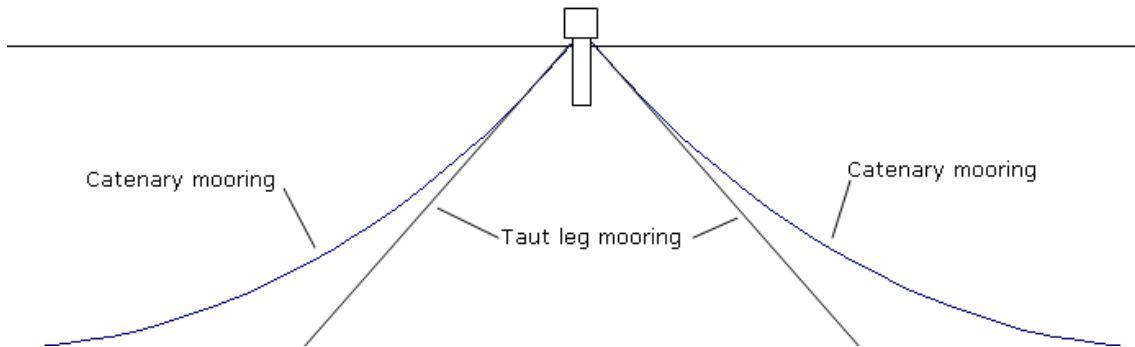


Fig. 6 – Schematic representation of catenary and taut leg mooring system.

In practical situations, mooring lines usually present hybrid behavior between the above-mentioned limit cases, as catenary mooring lines can become semi-taut or taut when the fairlead motion is such that the line is completely suspended, thus transmitting vertical loads to the anchors and modifying their static and dynamic responses based on axial stiffness. In addition, mooring lines generally contribute to the system overall dynamics through not only restoring forces, but also dynamic forces induced by interaction with waves, currents, seabed, etc. The choice of the scaling strategy for the mooring system of a floating structure is generally case-dependent, since the objective functions of interest and the impact of the mooring line parameters on them may vary. Extensive effort has been paid during the last years to quantify this impact on traditional structure concepts. This could serve as a basis to define the opportune scaling strategies for MPP mooring systems.

Barrera et al. [90] analyzed the importance of the main mooring lines parameters in the assessment of the mooring loads of a catenary line, using different numerical models and an experimental database. They figured out that line length has an enormous impact on mooring loads, as line tensions were doubled for length variations smaller than 1%. A smaller but still relevant importance was played by the line weight, the transverse and longitudinal drag coefficients and, to a lesser extent, the internal damping coefficient of the line. The latter two have a greater impact at higher frequencies, since they are associated with greater velocities. In this regard, it should be noted also that: 1) motions at the top end of the mooring are amplified geometrically in the lower sections; 2) the corresponding high drag resistance induces the line to behave elastically close to the fairlead at high frequencies. The latter phenomenon, also known as whipping, is extensively described in [88,91,92]. Finally, other parameters such as seabed characteristics, added mass coefficient and axial stiffness of the line (except for the snap load case, due to whipping or to semi-taut or taut line) were found to have a negligible effect on the loads. These results are widely confirmed by other studies, which highlighted as well, however, that the dynamic effects on mooring loads do not generally correspond to significant impacts on the coupled dynamics of floating platforms [93–97]. Among the others, e.g., Stansby et al. [95] and Hall and Goupee [96] showed numerically and experimentally that mooring forces and platform motions are largely decoupled for semi-submersible FOWTs, the latter being well-predicted by quasi-static mooring models. This is because mooring forces are generally significantly smaller than the other

contributions in the equation of motion of the floater. However, coupling between mooring and floating structure dynamics are relevant in some particular cases, especially when close-to-resonance behavior and second-order effects are of interest. This is the case of floating structures designed to resonate with first-order wave loads, such as floating WECs [88,91,98,99], and of dynamic analyses including low-frequency (LF) motions [88,100–102], since the long natural periods of horizontal motions may coincide with second-order wave loads, i.e. slow-drift forces and difference-frequency loads, thus inducing resonance. The importance of mooring lines dynamics generally increases with water depth [103–105], since the corresponding drag (and inertia) forces increase, whipping and snap loads become more likely and LF motions importance increases. It is worth mentioning that drag mooring line forces may represent a primary source of damping for floating structures, in particular when water depth is high (see e.g. [106]).

In the context of MPPs, it is important to emphasize that, unlike WECs, they are generally designed to avoid resonance with the 1st order wave loads, consistently with most of the subsystems' requirements. In addition, most of the MPP concepts are proposed for shallow or intermediate water depths at the present stage of research, since the cost increase in deeper waters (due to heavier mooring systems and greater distances from shore) is generally not yet sustainable. Concepts based on spar-type floaters may be an exception to the latter point, since they require relatively deep waters. It follows that simplified quasi-static scaling procedures may be often deemed acceptable for MPPs, as long as the precise reproduction of the mooring dynamics is not necessary. On the opposite side, full dynamic physical models should be used if LF motions, other close-to-resonance effects and/or line tensions must be represented. This choice depends also on the particular purpose of the test. For instance, approximate and conservative assumptions usually are acceptable in early-stage concept investigations, and simple linear horizontal moorings can be used for reproducing benchmark data for numerical simulations.

The most common quasi-static scaling strategies are based on the adoption of linear and nonlinear springs, opportunely calibrated to represent the force-displacement behavior of the mooring lines (see e.g. [107–110] and related references). Linear spring approach is inherently inaccurate for relatively large motions, thus introducing potential alterations in coupled dynamic representation, both in time [104] and frequency domains [111], particularly around the structure natural frequencies.

The ideal dynamic scaling of mooring lines is instead very complex. In the following, some theoretical and practical aspects are discussed, to provide guidance for future experimental activities. An up-to-date overview of the mooring system scaling procedures for general offshore structures is proposed by Bergdahl et al. [108], where also an extended literature review and critical discussion of the previous efforts in this field can be found. Based on dimensional analysis principles, they proposed a set of five parameters to achieve full dynamic similitude of a catenary mooring line, subject to oscillatory loads of period T . Alternative formulations can be found earlier in Papazoglou et al. [112], Webster [113] and Mavrakos et al. [103], who proposed sets of nine, twelve and nine dimensionless parameters, respectively. The five parameters proposed in [108] are:

$$\alpha_1 = \frac{C_a \rho_w}{C_v \rho_c}; \quad \alpha_2 = \frac{4KT^2}{C_v \pi D_c^2 \rho_c L^2}; \quad \alpha_3 = \left(1 - \frac{\rho_w}{\rho_c}\right) \frac{gT^2}{L^2}; \quad \alpha_4 = \frac{2C_d L \rho_w}{C_v \pi D_c \rho_c}; \quad \alpha_5 = \frac{2C_{d,l} L \rho_w}{C_v \pi D_c \rho_c}. \quad (11)$$

The first parameter α_1 is the ratio between added mass and structural mass of the cable, where ρ_w and ρ_c are the densities of the water and of the cable, respectively, and C_v is a volume coefficient, defined as the ratio between the unit volumes of the cable and of a cylinder with diameter D_c . The second parameter α_2 is the ratio between the propagation celerity of longitudinal elastic waves along the catenary line and the characteristic velocity, where K is the cable stiffness. It could be noted that α_2 represents the inverse squared Mach number of the problem. The third parameter α_3 is the ratio between the gravitational and inertial (added mass excluded) forces, hence it represents the inverse squared Froude number, as per Eq. (3), with a

correction factor related to the submerged weight of the cable. The fourth and fifth parameters α_4 , α_5 represent the ratio between transverse and longitudinal drag forces, respectively, and weight of the cable, where $C_{d,l}$ is the longitudinal drag coefficient of the cable. The drag forces are defined by means of Morison equation (Eq. 6), using the nominal diameter of the line. It should be noted that additional parameters would be needed to scale current and bending stiffness of the line [113], which has however a negligible impact for practical applications. Similarly, seabed characteristics are not taken into account. Interested readers may find extensive description of their effect on mooring dynamics and related scaling procedures in [92], even though these aspects may be neglected in most application cases. Eq. (11) refers to the similarity of the mooring line alone and is useful for dedicated experiments. However, for physical models of the coupled floater-mooring system additional constraints apply. In particular, the total wet weight of the line and the hydrodynamic forces must be scaled by the factor λ_L^3 . Since inertia forces of the mooring lines are negligible in most practical cases, two additional parameters can be obtained:

$$\alpha_6 = \frac{(\rho_c - \rho_w)C_V D_c^2}{L^2}; \quad \alpha_7 = \frac{\rho_w C_d D_c}{L}, \quad (12)$$

assuming a proper Froude scaling of the mooring line length and shape. It is evident that such ideal scaling cannot be achieved in practical cases. At full-scale, mooring lines are usually made up of wire ropes, chains and/or fiber ropes (see e.g.[88]), however scaled ones are generally not available on the market. As a consequence, decorative chains [27,108] or other opportune items are generally used instead, resulting in potential constraints on C_V , D_c and ρ_c . For the same reason, it is extremely difficult to achieve the desired axial stiffness, which is generally far smaller than those of decoration chains available on the market. The most common strategy to deal with the last issue is the insertion of a spring, in series with the model catenary line [92], calibrated so as to achieve the desired stiffness. This approach could be extended also to the case of multi-segmented mooring line, using multiple springs [103], but it is highly questionable because it does not allow representing correctly the occurrence of snap loads and introduces a natural frequency, which must not be close to the wave frequency range. It follows that the insertion of springs to model line axial stiffness is discouraged, and acceptable only in quasi-static framework, when axial stiffness is important for the line response (taut and semi-taut lines). Another very important issue is the unavoidable reduction of Re , affecting the drag coefficients of the mooring lines (variations of the added mass coefficient will not be discussed for the above-mentioned reasons). The problem is conceptually equivalent to the case of slender cylinders discussed in section 3.1, however mooring lines present a significantly different range of KC and Re of interest, as well as potentially non-cylindrical cross-sections (e.g. chain). Based on Fig. 4, Bergdhal et al. [108] proposed to use the steady flow curves also for chains subject to oscillatory flows, being KC generally very high, due to the very small diameter of the mooring lines. They highlighted at the same time, however, that this approach is not justified, as the chain shape is not cylindrical. Mavrakos et al. [103] observed that drag coefficients similarity could be deemed acceptable for $Re > 100$. This statement seems not shareable as well, since most studies show instead a huge variability of the drag coefficients, even in narrow Re ranges. Unfortunately, these dedicated studies are few and their results are often inconsistent, very scattered and of difficult interpretation. A tentative summary is reported in Table 2, with reference to both scientific literature and offshore standards currently available. In general, the following observations can be drawn:

- Drag coefficients generally tend to decrease with Re , in line with the case of slender cylinders. They are hence expected to be smaller at full-scale with respect to model scale. This effect could be compensated by altering (narrowing) the scale factor of D_c to match drag forces as well as possible in a given Re range, by means of Eq.13. The equation is based directly on Eq. 6, and the terms have the same meaning, “p” stands for prototype and “m” for model. The main limitations of this approach are: 1) the chosen Re range generally corresponds to a limited of wave/structure motions of the full-scale structure; 2) it alters inertial forces, hence it is admissible only to represent drag-dominated

phenomena (e.g. drag damping estimations in LF motions); 3) the resulting diameter could be too small, resulting in structural resistance and/or commercial availability issues.

$$\lambda_{D_c} = \lambda_L \frac{C_d(\text{Re}_m)}{C_d(\text{Re}_p)}; \text{Re}_p = f(D_{c,p}, \mathbf{v}, \dot{\mathbf{x}}); \text{Re}_m = \text{Re}_m \lambda_{D_c} \lambda_L^{0.5}, \quad (13)$$

- Data scatter is larger for chains compared to ropes, particularly for very small scales (small Re).
- Drag coefficients estimations from experiments generally embody also other effects, such as the internal damping of the line.
- Care should be taken to the arbitrary definition of the nominal line diameter for non-cylindrical cross sections, since it may vary from case to case, affecting the value of the drag coefficient.
- Further experimental campaigns at model and full scales are required to support the drag coefficient estimation and provide reliable and consistent data, especially for ranges of values typical of MPP chains, which are smaller than oil & gas applications.
- Real drag forces in operational conditions are highly uncertain, also because of marine growth and other random phenomena, occurring during the structure life. It is then reasonable to assume full roughness when designing scale tests. Although uncertainty is a key feature of any damping force, it is particularly remarkable for mooring systems, making somehow questionable the requirement of detailed representations of these forces through physical models.

Ref.	Method	Re range	C_d range	Notes
[114]	Measured	~40	~3.00	Chain; $D_C = 1.05$ mm; towing
		~90 to ~200	~2.60 to ~2.20	Chain; $D_C = 1.05$ mm; towing
		~ $6.0 \cdot 10^3$ to ~ $1.1 \cdot 10^4$	~2.90 to ~2.30	Chain; $D_C = 30$ mm; KC range = 163 to 306
		~ $1.3 \cdot 10^4$ to ~ $4.0 \cdot 10^4$	~2.80 to ~2.50	Chain; $D_C = 30$ mm; towing
		~ $4.0 \cdot 10^4$ to ~ $1.8 \cdot 10^5$	~2.70 to ~1.65	Chain, stud; $D_C = 65$ mm; towing
		~ $9.0 \cdot 10^4$	~1.55	Chain; $D_C = 30$ mm; towing
[115]	Measured	~180 to ~ $1.9 \cdot 10^3$	~4.00 to ~0.60	Chain; drop test, $D_C = 3.4$ mm; large scatter for given Re .
		~220 to ~ $1.9 \cdot 10^3$	~2.80 to ~0.50	Chain; drop test, $D_C = 4.1$ mm; C_d seems to increase with Re in the mid-range; large scatter for given Re .
		~450 to ~ $2.6 \cdot 10^3$	~1.98 to ~1.12	Chain; drop test, $D_C = 4.8$ mm; large scatter for given Re .
		~450 to ~ $6.4 \cdot 10^3$	~0.50 to ~1.68	Chain; drop test, $D_C = 5.84$ mm; C_d seems to increase with Re in the low-range; large scatter for given Re .
		~ $3.5 \cdot 10^3$ to ~ $2.6 \cdot 10^4$	~0.92 to ~1.80	Chain; drop test, $D_C = 19.54$ mm; C_d seems to increase with Re ; large scatter for given Re .
[105]	Numerical (CFD)	~ $7.5 \cdot 10^3$ to $3.0 \cdot 10^5$	2.55 to 2.25	Chain, stud-less; potential inaccuracies for higher Re values; KC not considered
[65,116]	Measured, transv. C_d)	13 to 110	3.00 to 2.50	Chain; $D_C = 1.05$ mm; towing
		13 to 120	2.50 to 1.80	Chain; Scale between 1:200 and 1:55
		$1.4 \cdot 10^3$ to $1.0 \cdot 10^4$	2.70 to 2.10	Chain; $D_C = 30$ mm; KC range = 163 to 306
		$1.0 \cdot 10^4$ to $1.3 \cdot 10^4$	2.70 to 2.20	Chain; $D_C = 30$ mm; towing
		$1.3 \cdot 10^4$ to $1.1 \cdot 10^5$	2.50 to 1.70	Chain; $D_C = 65$ mm; towing
		$1.05 \cdot 10^5$	1.4	Chain; $D_C = 147$ mm; velocity = 1 m/s
		11 to 140	2.00 to 1.00	Wire rope; $D_C = 0.65$ to 3.00 mm; towing
		13 to 120	1.10 to 0.90	Wire rope; Scale between 1:200 and 1:55
		120 to 14000	0.80 to 1.10	Wire rope; $D_C = 1.10$ to 3.80 mm; towing
		104 to $1.4 \cdot 10^4$	1.10 to 0.95	Wire rope; $D_C = 1.10$ to 3.80 mm; drop test

		1.4·10 ⁴ to 1.1·10 ⁵	1.05 to 0.90	Wire rope; $D_c = 78$ mm; towing
		1.0·10 ⁵	0.83	Wire rope; $D_c = 147$ mm; velocity = 1 m/s
	Proposed values (2-D, transv. C_d)	1.0·10 ⁴ to 1.0·10 ⁷	2.20 to 2.60	Chain, stud
			2.00 to 2.40	Chain, stud-less
			1.50 to 1.80	Wire rope, six strand
			1.40 to 1.60	Wire rope, spiral, no sheathing
			1.00 to 1.20	Wire rope, spiral, with sheathing
[117]	Proposed values	No indications	2.60	Chain, stud, transv. C_d
			1.40	Chain, stud, longit. C_d
			2.40	Chain, stud-less, transv. C_d
			1.15	Chain, stud-less, longit. C_d
			1.80	Wire rope, stranded, transv. C_d
			1.60	Wire rope, spiral, no sheathing, transv. C_d
			1.20	Wire rope, spiral, with sheathing, transv. C_d
			1.60	Fibre rope, transv. C_d
	0.00	Longit. C_d for ropes (stranded, spiral with and without sheathing and fibre)		
[115,118]	Other measured data			

Table 2 – Drag coefficient estimations deduced by available scientific studies and offshore standards, under oscillatory and steady flow conditions.

Another key point in mooring lines scaling is the water depth and footprint available. They are indeed inherently limited in indoor laboratories, which may not be compatible with the Froude scaling of the line length and shape, at the desired scale factor. This could be a relevant problem for MPP applications, where scale factors should be kept as small as possible to scale opportunely all the subsystems involved. In these cases, the most suitable scaling strategy is the truncation of the mooring lines, which is common in oil & gas physical models. The most common truncation strategies are based on the design of the truncated line within a quasi-static framework, through the use of empirical formulae (see e.g. [119,120]) or more time-consuming and accurate optimization algorithms (see e.g. [121]). This could be conceptually regarded as a subcase of the nonlinear spring approach, since the truncated lines are designed to reproduce the static force-displacement relationship of the original ones, but leaves also room for improvement in the representation of the dynamic loads. To this purpose, several hybrid strategies have been proposed (see e.g. [40,121]): use of viscous dampers [122] or actuators [123] for the representation of the dynamic forces on the truncated segment; increase of the truncated line diameter to opportunely compensate the reduction of drag loads, while keeping the line wet weight from quasi-static optimization algorithm [124]; etc. If hybrid strategies involving auxiliary numerical tools are to be implemented (e.g. Hardware-In-the-Loop techniques), the characteristics of such models should be carefully taken into account. Especially, the computational cost must be compatible with the real-time loop [125]. Although truncation could be very effective either for catenary, semi-taut and taut moorings [126], great care should be taken, particularly for MPP applications, as the inaccuracies unavoidably introduced through truncation may be very relevant. A relevant example is that of slender MPPs: if their draft is highly sensitive to the total wet weight of the mooring system, quasi-static optimization algorithms based on the horizontal motions reproduction could result in non-negligible draft alterations, which in turn alter the overall MPP dynamics (wave forces, restoring moments, natural periods, etc.) [121]. This applies also if an additional mass is used to restore the original equilibrium position.

The opposite case of mooring truncation may take place in outdoor experiments, if the inclined seabed makes the operational water depth for certain lines higher than the required one [27]. In such a case, however, the same optimization and verification methods discussed for truncation should be used, except for hybrid strategies, which usually result practically unfeasible at sea due to the system complexity and costs+. In addition, when operating at sea, local extreme conditions must be taken into account, since they may exceed

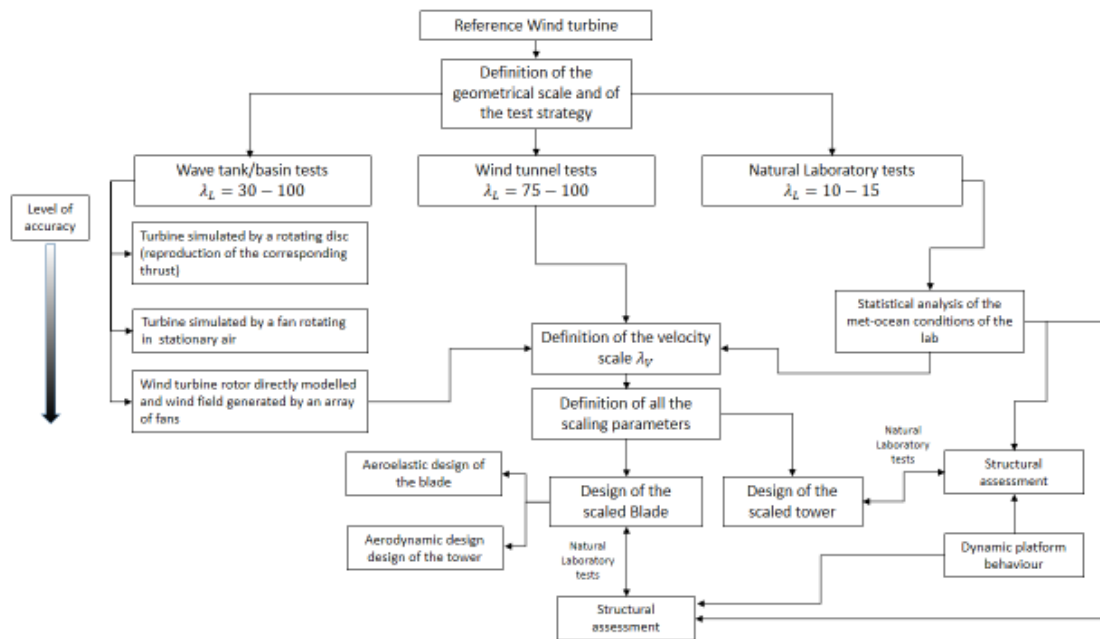


Fig. 8 – Proposed schematic workflow for the design of scaled wind turbine.

3.3.1 Tests in wind tunnel

For wind tunnel testing of wind turbines, a proper geometrical scale for the model can be selected in consideration of the wind tunnel dimensions. In particular, the largest scale that permits to neglect blockage effects is generally chosen in order to avoid excessive miniaturization of the model components. The scale is also chosen to opportunely reproduce the full-scale wind profile, i.e. the variation of mean wind velocity and turbulence with height at model scale. For offshore applications, the reference wind profile typically adopted is the Eurocode 1 [127] that refers to sea or coastal areas in wind engineering design.

The wind turbine model components can be designed following different strategies. In particular, different needs have to be taken into account considering the three subsystems: 1) tower; 2) nacelle; 3) rotor. The tower shape can be easily obtained geometrically, scaling the reference one. If aero-elastic design would be required, the material and internal structure will be selected in order to properly reproduce its first fore-aft mode frequency and shape. In scaling the tower characteristics, Froude scaling approach is used. The nacelle is designed trying to properly scale the global masses and to grant the main required functionalities: as the mechanical components cannot be miniaturized at will, the respect of the functionalities is considered a stricter constraint. The rotor design is more complex and deserves a specific approach, different from the one used for typical wind tunnel applications.

Given the length scale factor λ_L , all the other factors can be derived fixing the velocity scale factor. The incompatibility between Froude and Reynolds scaling sets a major constraint for experiments that require to physically scale the complete floating structure. If Froude scaling is used, scale factors between $\lambda_L = 50-100$, required to fit a multi-megawatt wind turbine in a common testing facility, lead to velocity scale factors $\lambda_V = 7-10$ and Reynolds numbers Re between 350-1000 times lower than the one experienced by the full-scale system. This is problematic for scaling of the wind turbine rotor and for the correct reproduction of aerodynamic loads. Wind tunnel hybrid/Hardware In the Loop (HIL) experimental methodologies were proposed as a potential solution to the Froude-Reynolds conflict, making possible to correctly reproduce the wind turbine aerodynamics and its effect on the coupled system dynamics in scale model experiments [24]. The adoption of the HIL methodology relaxes the scaling constraints and allows neglecting the Froude scaling approach, due to the absence of physical gravitational-based forces. Hence, length and velocity scale factors

can be set independently, keep instead similar Tip Speed Ratio (TSR) between model and full scales. TSR is defined as the ratio between the tangential velocity at tip due to the wind turbine rotation and the wind velocity. TSR similitude ensures to have the same aerodynamic kinematics and working condition for the reference and model turbines. Moreover, in the rotor design of a FOWT, it is worth mentioning that the thrust matching is of higher importance than torque, since it influences the floating system dynamics more significantly [128]. This is the so-called “performance scaling” approach, that consists in a redesign of the blade geometry in order to obtain the scaled thrust force, at the scaled wind speed. This approach is consistent with the STAGE framework, as the thrust is the main turbine item in the governing equations of motions of the floater. In this context, the main goals in the blade design are: 1) matching the reference thrust coefficient; 2) Matching the scaled blade weight. If also the dynamic characteristics of the blade represent a target, i.e. an aero-elastic model is required, matching the scaled first blade flapwise natural frequency is a further goal to be achieved. In this case, the aerodynamic and structural optimization should be carried out iteratively, until the design reaches an optimal solution. The blade re-design is due to the unavoidable lack in Reynolds Number between model and full scales (a Reynolds scaling approach would result in an unfeasible flow condition for wind tunnel facilities for the considered scale factors): in order to obtain a suitable thrust a proper airfoil profile, tuned on the experiment Reynolds number range, must be adopted. As stated in [129], the characteristic airfoil profile for a blade has a suitable behavior if its lift coefficient curve, as a function of the angle of attack, is characterized by a wide linear trend at the Reynolds number of the tests. This permits to keep the wind turbine operating conditions far from the stall at both model and full scales. Once the proper airfoil profile is chosen, a complete 3D design of the blade can be obtained using numerical tools, such as FAST [130], as support.

3.3.2 Tests in wave tanks/basins

Model tests of floating wind turbines in wave tank/basin have been extensively reported in literature, since the modelling in scale of the wind turbine aerodynamics is identified as one of the most significant challenge, due to the conflicts between Froude and Reynolds scaling. Several approaches, of increasing accuracy and complexity, are reported in the following.

Simulating the steady wind load using a weight should be avoided, since it may substantially alter inertia of the system, and should only be used to estimate (approximately) the maximum mooring offset [131]. A solid disc and a battery of fans can be used to generate a drag load corresponding to the thrust on the turbine. Scaled rotary moment of inertia can be achieved with a rotating disc or a separate rotating arm, to model the gyroscopic coupling between the rotor and the platform [132]. In general, this approach is considered quite approximated, since it is aimed only at having a first estimate of the platform response to the aerodynamic thrust force, but does not reproduce the complexity of the aerodynamic loads acting on the wind turbine. Alternatively, another approach suitable for small-scale tests where a low accuracy is sufficient to assess design in the conceptual stage, is to use of a fan rotating in an otherwise stationary air [133]. This ensures a higher level of accuracy with respect to the previous approaches, since the mean wind load can be easily adjusted, and it overcomes the need for an expensive wind generation system. As limitations, it is difficult and sometimes not possible to reproduce the correct mean thrust, mean torque, and tower interaction effects, and the gyroscopic effect may be wrongly represented. The direct modelling of the wind turbine rotor has been investigated by a number of authors (see e.g. [131,134,135]), by using a wind field generated by an array of fans and a rotating rotor, the last in geometrical scale or scaled following alternative approaches. A correct scaling of the wind field shear and turbulence are usually very challenging to achieve, also considering the presence of a wavy water surface. Alternative to the geometrical scaling of the rotor, is the “performance scaling”, i.e. scaling the rotor in such a way that the thrust curve and the inclining moment of the wind turbine are correctly scaled when using the Froude-scale approach [128,129,136], over a range of wind speeds. This is achieved by changing the geometry of the blades. Li et al. [137] proposed the free rotation approach and implemented it in the model test conducted in the Deepwater Offshore Basin at

Shanghai Jiao Tong University. Although the desired thrust force was obtained, the TSR was not exactly maintained.

Recently, hybrid/HIL (Hardware In the Loop) model testing approaches have been proposed also in this context [138], primarily to overcome the conflicting requirement of Froude and Reynolds scaling. In a complementary way with respect to wind tunnel case, the wind turbine is modelled numerically, and linked in real-time with a subsystem realised physically through an experimental model. An example of this is having a numerical simulation to derive the aerodynamic loads acting on the FOWT system, and therefore reproducing at synthetic level also the wind field, and then apply these loads (through suitable actuators) to a physical model of the floating support structure in a conventional wave basin. A simple approach [139] is to use a fan driven by an electronic motor, which is linked to a proper time-domain software package, able to take as input the instantaneous position and velocity of the physical support in the basin, and output the corresponding aerodynamic thrust force to be transmitted by the RNA to the support structure. Complex and strong wind fields, as well as rotor and blade control strategies, can be included in the evaluation of the thrust force, and this is a strong advantage with respect to the previous approaches. This hybrid technique has been also adopted for testing multi-purpose platforms by the authors [140]. An alternative approach, overcoming the limitation of being able to reproduce only the aerodynamic thrust, has been proposed by Sauder et al. [141] and Bachinsky et al. [142], using cables and actuated winches to reproduce the forces transmitted by the RNA to the floating support structure in five degrees of freedom. The overall main limitation of the hybrid model testing is that the loads calculated at numerical level can be as accurate as the numerical approach adopted, or less. Therefore, although its substantial advantages have been proven in several studies, they will not be able to achieve the same accuracy of a properly scaled physical model, since the unknown phenomena that can arise with novel concepts, by definition, are not captured by existing numerical approaches.

3.3.3 Tests in field laboratories

For an outdoor model design, a compromise between this scaling rule and all the requirements related to the interaction between the prototype and the real-life environment in the laboratory area must be considered (e.g. environmental impact assessment). A further complication is related to the met-ocean conditions of the test site. Differently from traditional indoor laboratory tests, wind-wave input cannot be controlled and the expected conditions must be considered in the model design process in probabilistic terms. Moreover, as the interdependence of wind-waves at the test site could be not representative of the target deployment site, a compromise in defining the scaling parameters for hydrodynamic and aerodynamic phenomena should be found [13]. In order to define the wind velocity scale factor, the cumulative distribution functions of the full-scale deployment site and field laboratory have to be compared. This criterion ensures the same probability to have the wind turbine working in partial or full-load conditions for both model and prototype. An acceptable length scale for a multi-megawatt wind turbine is set within the range 1:10-1:20. This allows a better reproduction of the turbine aerodynamics with respect to smaller scale wind tunnel tests and, at the same time, it permits to limit the dimensions of the whole MPP physical model. Once the length and velocity scale factors are defined, the other parameters are defined applying Froude scaling approach, in particular to scale the thrust force acting on the rotor, the masses and the tower aero-elastic parameters. As for an indoor model, the blades shape must be re-designed as a simple geometrical scaling would not permit to obtain the same performances of the full-scale due to the above-mentioned difference in Reynolds numbers. Hence, "performance scaling" must be applied. As described in [17,18], the criteria used for the design of an indoor wind turbine model must be completed with safety and structural requirements of real turbines. In particular, some constraints in the rotor dimension could be introduced to reduce costs, facilitate the design and the installation. Moreover, applicable standards (see e.g. [143]) must be applied, in order to grant the structural integrity and a safe functioning, as for a real structure. Environmental impact should be taken into account as well, when applicable. From the standards, static load

cases can be identified and applied, in order to verify the machine in operation and extreme wind conditions. For offshore structures, also the excitation related to the sea must be taken in consideration in the structural design, considering the effects of the mean and the extreme events. Moreover, dynamic loads have to be included in the structural assessment of a floating wind turbine model, as the platform displacement can induce important solicitation in the model. In [48], an example of large model in natural environment is described.

3.4 Wave Energy Converters

Embedding wave energy converters in MPPs is an obvious choice: the structures are surrounded by an energy-wise rich field, that can be exploited by an infrastructure able to host the requested mechanical and electrical equipment. Moreover, their capability of subtracting energy from the wave field makes them an option also for attenuating the coupled system response [144]. A variety of WECs is described in the open literature, but only a few proved to be effective in full-scale tests. In particular, single point absorbers, overtopping devices and oscillating water columns (OWCs) are the most promising from an energy – wise perspective [145]. In this context, OWCs are probably the most natural choice for the designers. Indeed, they can be embedded easily in the geometrical configuration of the MPPs, without sacrificing significantly operation and maintenance of other subsystems. Their configuration comprises a chamber with a water column, an air pocket on top of it and a Power Take Off (PTO) system. The sea waves excite the water column, thus inducing oscillations of the inner free surface. Such oscillations compress and decompress the air pocket, which in turn activate the PTO and generate electrical energy. Relevant applications in coastal areas (mainly in conjunction with upright breakwaters) proved their reliability from both a structural and an energetic perspective [146,147]. Positive effects were observed also in the context of floating structures. For instance, Hong et al. [148] showed numerically that an adequate design of a floating breakwater embedding an OWC can reduce significantly the response (deformation) of a protected VLFS. Similar observations were reported in experimental investigations involving simpler systems composed by OWCs in floating breakwaters only [149,150]. Instead, single point absorbers commonly do not interfere significantly with the surrounding wave field, because they are much smaller than typical wavelengths. Thus, they are not able to reduce the wave action on a nearby structure. Finally, overtopping devices could potentially lead to unsafe operative conditions, as they are supposed to magnify the wave run-up on the structure for accommodating the storage of water above the mean water level.

In general, OWC testing is planned by exploiting the DA concepts elucidated in section 2. In this framework, OWC tests are conducted initially at a small scale ($\lambda_L = \sim 100$ to ~ 10) in indoor laboratories. Then, they are tested possibly also at an intermediate/large scale ($\lambda_L = \sim 4$) outdoor, in confined or protected natural basins characterized by scaled sea states compatible with the ones at the installation site [48]. The model testing procedure of an OWC revolves around the three elements composing the WEC: 1) the water column; 2) the air chamber; 3) the PTO system. These three systems cannot be fully integrated in one common scaled framework directly (in this regard, a comprehensive discussion about the OWC testing procedures was given by Falcão and Henriques [19]).

The sea states and the water column are scaled in Froude similarity. Considering the fact that the water column behavior is commonly modelled in the framework of linear water wave theory, the scaling laws given in Table 1 are applicable without significant efforts. However, the representation of the air spring-like effect on the water column is a daunting task. The main problem relates to the fact that model and prototype air chambers are both operating at the same atmospheric air pressure. This issue was described in details by Falcão and Henriques [151]. Specifically, considering the equation of conservation of the air mass, they showed that for preserving the dynamic similarity the following equation holds:

$$\frac{V_m}{V_p} = \frac{q_m (p_{c,m} + p_{atm,m}) \left[\frac{dp_c}{dt} \right]_p}{q_p (p_{c,p} + p_{atm,p}) \left[\frac{dp_c}{dt} \right]_m}, \quad (14)$$

where V is the air chamber volume, q is the air volume flow rate, p_c is the air pressure, p_{atm} is the atmospheric pressure and the subscripts “ m ” and “ p ” denote quantities pertaining to the model and to the prototype, respectively. Therefore, in Froude similarity, the scaling factors associated with the related physical parameters are:

$$\lambda_V = \lambda_L^3; \quad \lambda_q = \lambda_L^{2.5}; \quad \lambda_{p_c} = \lambda_{p_{atm}} = \lambda_{\rho_w} \lambda_L; \quad \lambda_{\frac{dp_c}{dt}} = \lambda_{\rho_w} \lambda_L^{0.5}, \quad (15)$$

where water density ρ_w may vary from prototype to model if sea water ($\rho_w = \sim 1025 \text{ kg/m}^3$) is used in place of fresh water ($\rho_w = \sim 1000 \text{ kg/m}^3$).

It is obvious that the condition on p_{atm} scale factor dictated by Eq. 14 is impossible to be satisfied, unless going to close to prototype scales, i.e. $\lambda_L \approx 1$. For circumventing this issue, the pressure oscillations p_c are assumed negligible compared to the atmospheric pressure p_{atm} . This approximation excludes the possibility of testing extreme sea states in Froude similarity, but, by considering also that $p_{atm,m} = p_{atm,p}$, it provides a different scale for the chamber volume:

$$\lambda_V = \frac{\lambda_L^2}{\lambda_{\rho_w}}, \quad (16)$$

This means that scaled testing can be conducted by utilizing a “deformed” air chamber model. This approach to OWC testing was utilized for the physical model tests of the Pico OWC plant in Lisbon (Portugal) and in Cork (Ireland) [152]. In practical implementations, larger air chambers at model scale are needed. They are realized by connecting the scaled air chamber to a reservoir through a connecting pipe. In the test of fixed OWCs this configuration does not pose specific problems. Indeed, it is sufficient to guarantee that the pipe does not introduce relevant pressure losses. In contrast, it can be difficult to use it for testing floating OWCs. Indeed, in that case, the reservoir and the connecting pipe might induce unexpected forces and moments on the floating body, that might give rise to altered dynamic response. In this circumstance, one option could be the use of highly flexible pipes connected to a fixed reservoir [153]. However, this approach is useful only in indoor tests, where a support for the external reservoir can be made available, but it seems quite difficult to apply in outdoor tests. In this context, the main problem relates to the fact that the reservoir must be installed on the floating body itself. Therefore, the mass distribution of the whole floating body is inevitably altered and may not be representative of the prototype configuration. Clearly, this problem affects mainly the small floating structures. However, also large floating platforms, such as some MPPs, are exposed to similar issues. Indeed, installing additional reservoirs alters not only the mass distribution, but it constrains also the MPP space utilization, which may be a serious issue in the simultaneous test of various technologies.

The PTO system implemented in conjunction with OWCs is commonly a self-rectifying air turbine. In this context, the classical Wells or impulse turbines have been tested deeply in the literature [154]. Nevertheless, other technologies were developed and tested, such as the Dielectric Elastomer Generators [155].

The turbine testing is not conducted in conjunction with the OWC small scale models. Instead, the systems are physically coupled only in the large-scale tests. The problem relates to the fact that the performance of a small-scale turbine is not representative of a full-scale one. In this context, the application of the Buckingham’s theorem allows establishing a dependence of the dimensionless flow rate across the turbine and the turbine power output of the form [151]:

$$\Phi, \Pi = f\left(\frac{p_{0,in}}{p_{out}}, Re, Ma, \frac{c_p}{c_v}\right), \quad (17)$$

where

$$\Phi = \frac{|w|}{\rho_{0,in} \Omega D_t^3}, \quad (18)$$

$$\Pi = \frac{P_t}{\rho_{0,in} \Omega^3 D_t^5}, \quad (19)$$

in which: Ω is the turbine rotational speed; D_t is the turbine diameter; the subscripts “0,in”, “out” denote turbine entry in stagnation conditions and static conditions at turbine exit, respectively; Φ is the dimensionless flow rate; Π is the dimensionless power output; P_t is the turbine power output; w is the air mass flow rate; c_p and c_v are the specific heat at constant pressure and at constant volume, respectively. The use of Reynolds number and Mach number is quite common in turbo-machinery, as they are used to quantify the relevance of viscous forces with respect to inertial forces and the relevance of compressibility effects. However, scaling by adopting these parameters is difficult, because the small scale turbines would operate at very different Re and Ma , with respect to their full-scale counterparts. So that, it is not possible to conduct tests with equal non-dimensional parameters. Therefore, small tests are simply avoided and the testing procedures are conducted at least on intermediate-scale turbines. In this context, Re and Ma are assumed irrelevant and the thermodynamic process in the chamber is assumed isentropic. Then, the power output and the air flow rate are dependent only on the dimensionless pressure Ψ , defined as:

$$\Psi = \frac{|p|}{\rho_{0,in} \Omega^2 D_t^2}, \quad (20)$$

while the ratio $c_p/c_v = 1.4$.

Despite the impossibility of testing directly small-scale turbines, their effects on the OWC dynamic response can be included in the model testing. For this purpose, the functional relation between dimensionless air flow rate and dimensionless pressure determines the approach to be used. In this context, it is important to make a distinction between linear and nonlinear turbines. The Wells turbines are considered linear, as they are characterized by a linear $\Phi - \Psi$ relation, while the other turbines, such as the impulse turbines, are characterized by a nonlinear $\Phi - \Psi$ curve. Specifically, impulse turbines have a quadratic relation. Therefore, the air mass flow rates across the turbine are given by equations of the form

$$\frac{dm_t}{dt} = k_l (p_c - p_{am}), \quad (21)$$

for the linear turbine; and

$$\frac{dm_t}{dt} = k_{nl} \sqrt{|p_c - p_{am}|} \text{sign}(p_c - p_{am}), \quad (22)$$

for the quadratic one, k_l and k_{nl} being constants. Eq. (21) shows that effects of the linear turbine can be incorporated by using a porous layer in the small-scale model orifice, as they are known to induce linear dissipations, while Eq. (22) shows that effects of quadratic turbines can be incorporated by a simple orifice. Determining the characteristics of these surrogate experimental PTO replacements can be in some cases a daunting task. The nonlinear turbine behavior is reproduced by designing appropriately the orifice diameter. Specifically, the diameter is determined by ensuring similar damping characteristics between the model and

prototype. In this context, it is seen that the damping is only slightly dependent on the turbine rotational speed. Therefore, there is no need for mechanical elements connected to the orifice. Instead, the replacement of a Wells turbine requires a more complex system. The mentioned porous layer must be designed for ensuring similar damping characteristics between model and prototype, but it should also include control valves controlling the porous layer open diameter, in order to reproduce the turbine behavior at a given rotational speed. The former approach is quite common in OWC testing and has been widely applied in the past, because it is quite straightforward to implement, but Falcão and Henriques [151] emphasized that it is a rough representation of the turbine effect that cannot replace, in any case, the need for full-scale tests.

The difficulties in volume and PTO scaling has led to the execution of experimental campaigns involving mainly geometrically scaled OWCs [156,157]. To the authors knowledge, the use of a deformed air chamber in floating OWCS was proposed only in [153]. These authors constructed a reliable scaled model by installing the additional reservoir on a fixed supporting structure. The connection between the model and the reservoir was done by a quite flexible pipe. Other experimental activities on floating OWC systems utilized only geometrical scaling or no scaling at all. In the last case, the experimental activity is devoted to the validation/calibration of an associated numerical model. For instance, Gomes et al. [158] proposed a time domain model of a Spar-Buoy OWC, which was validated by data from wave flume model tests. Their experimental activity emphasized the fact that the time domain model may not be able to describe properly the system dynamics in case of parametric resonance. Elhanafi et al. [159] used physical model tests for validating the 3D CFD model of an offshore floating moored OWC, which showed an improved power efficiency due to the surge motion of the floating device. Singh et al. [160] investigated the behavior of a TLP-type floating OWC under the action of extreme waves and observed that the hydrodynamic efficiency of the OWC was negatively affected by the floating body motion.

An indoor experimental test on a multipurpose platform comprising both OWCs and wind turbines was conducted by Sarmiento et al. [161] on a 1:35 model. They adopted a Froude scale to set up the experimental tests, while conceptualizing the OWCs by holes with simple openings in the structural layout.

In conclusion, a schematic visualization of the scaling procedures discussed in this section, relative to OWCs embedded in MPPs, is shown in Fig. 9.

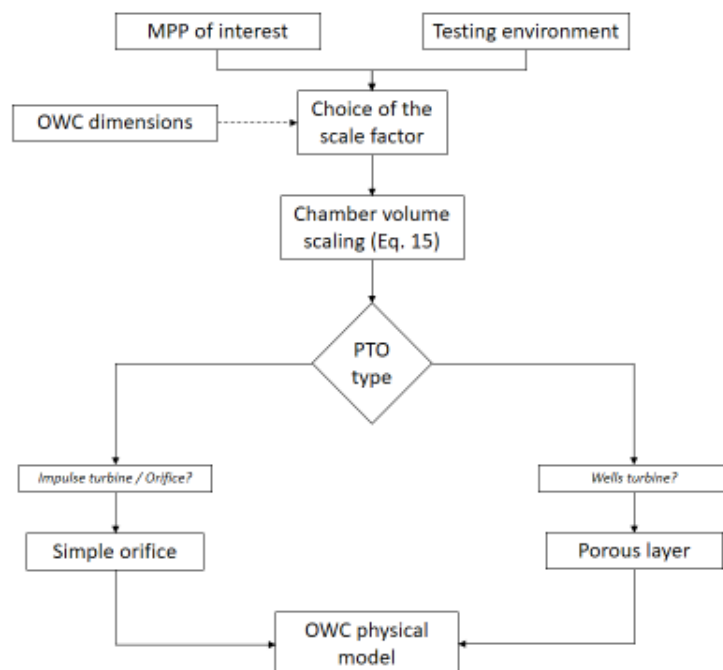


Fig. 9 – Proposed schematic workflow for the design of scaled OWCs within MPPs.

3.5 Fish net cages

The development of offshore aquaculture represents a key objective of the Blue Growth European strategy and collect interest from all over the world, as it would meet the growing requirement of sustainable food production, while reducing the inland/coastal space occupation. Standalone floating cages are already used in coastal areas for fish farming and may be of different types (see e.g. [162–164] for historical to recent reviews). In general, an open flexible cage system, also known as gravity-type cage, is made up of a containment net suspended between a floating collar and a sinker tube. The net is made up of square or hexagonal meshes ($\sim 5\text{--}50\text{ mm}$), assembled on a frame of vertical and horizontal ropes, arranged to collect dynamic efforts from net panels, and transmit them to the floating collar and the sinker tube. The twine diameter usually ranges between 1-5 mm for textile nets. The sinker tube is adequately ballasted, and connected to the collar by suspension ropes. A schematic representation of such flexible cage system is shown in Fig. 10. Rigid cage systems can be also used, where sinker and suspension ropes are substituted by a rigid frame, while closed systems with artificial water recirculation systems are rarer. The cage is moored to the seabed with chain, ropes or tendons.

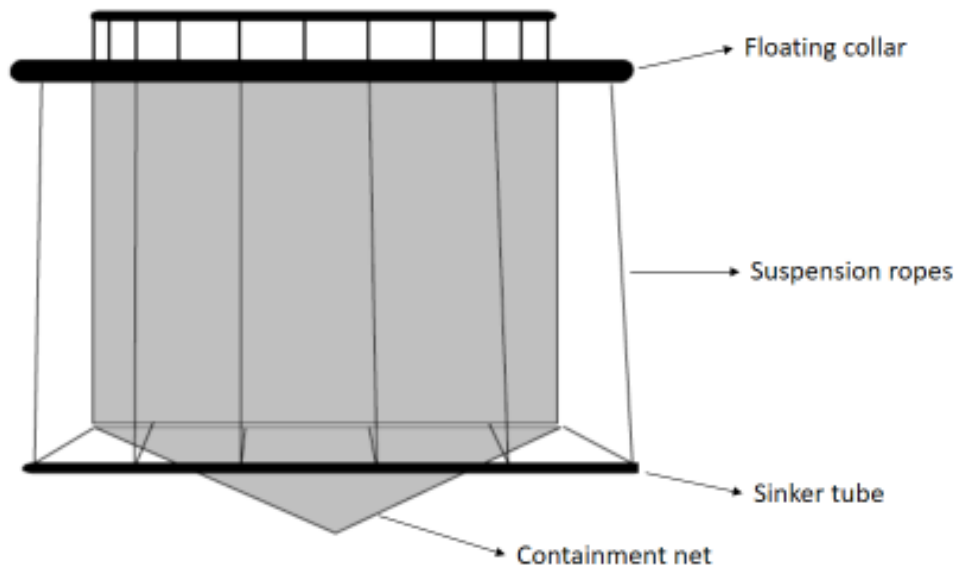


Fig. 10 – Schematic representation of a standalone open flexible floating cage system.

Offshore aquaculture cages are extremely promising for integration in MPPs for several reasons: 1) would receive protection from environmental loads, thus becoming feasible in more exposed offshore areas; 2) could share some functional elements with other subsystems, e.g. floater and mooring system; 3) could exploit local energy production from renewable sources, e.g. for automation; 4) could contribute to the overall MPP damping.

The scaling of aquaculture cages is a very challenging task. Their dynamic behavior is indeed complex, and still largely uncertain from quantitative and sometimes qualitative points of view [165]. It depends mostly on elastic and viscous phenomena, which cannot be scaled by means of Froude scaling laws. In addition, some elements (e.g. twine) are so small that direct scaling is impossible or at least impractical. However, slight simplifications apply when the cages are integrated within MPPs, since some elements, such as floating collar and mooring system, may become unnecessary, being substituted by the corresponding ones of the MPP. In this case, the cage contribution to the overall dynamics mainly regards the hydrodynamic forces on the net and the sinker weight and flexibility.

To accurately represent the hydrodynamic behavior of a cage, two characteristic length scales must be taken into account, i.e. those of the global cage and the local twine diameter. Both elements shed vortices, which

appear to have similar importance for the global response. Turner et al. [21] argued that similarity of the cage would be achieved if: 1) geometric similarity is respected; 2) shape of the cage is preserved; 3) streamline patterns are geometrically similar in the fluid domain inside and outside the cage; 4) velocity and pressure distribution are similar; 5) force coefficients are the same. This would require the simultaneous equality of Froude, Reynolds, Strouhal and Euler number, as defined in Section 2.2, for both characteristic length scales. It is clear that this ideal situation can be achieved only at full scale, hence approximate strategies must be adopted for the design of physical models, based on the understanding of the physics of the water-cage interaction phenomena (STAGE approach).

In MPP framework, hydrodynamic forces on the net are the main parameter of interest for the scaling, as they represent the interface between the cage system and the platform. Clearly, the forces depend on the global size of the mesh (diameter, depth, shape) [166,167], which must be scaled according to Froude laws. The mesh properties are instead impractical to be scaled directly, due to the small dimensions of the twine. It is hence useful to refer to numerical methods for the modeling hydrodynamic forces, which may be of Morison-type or screen-type [168]. The former approach (Eq. 6) simply sums the force contributions coming from each twine and knot and is clearly not feasible for STAGE scaling, since it is not possible to scale single lines, as already pointed out. The latter, instead, regards the net as a panel, calculating viscous forces as proportional to the area of the net panel. This approach allows also taking implicitly into account twin-to-twin wake effects. In this case, the force coefficients depend on a dimensionless parameter, namely solidity ratio, defined as the ratio between the projected net area on the “panel” and its total area:

$$S_n \equiv \frac{4(l_w - d_w) \frac{d_w}{2} + 4 \left(\frac{d_w}{2} \right)^2}{l_w^2} = 2 \frac{d_w}{l_w} - \left(\frac{d_w}{l_w} \right)^2, \quad (23)$$

where d_w and l_w are the diameter and length of each twine (square cage shape case), respectively. Some studies refer equivalently to porosity P , defined as the complementary of S_n . It is then common practice to keep S_n constant in scaling, to achieve force similarity (see e.g. [21,166,169,170]). However, as shown in the previous sections, viscous forces generally depend also on KC and Re , hence this scaling strategy may not be sufficient. Due to the very small twine diameter, inertial forces are generally regarded as negligible with respect to viscous ones (see e.g. [168]) and KC values are very high, resulting in negligible influence on hydrodynamic coefficients [169,171]. Differently, the influence of Re is often non-negligible, as larger drag and lift coefficients C_d , C_l could result from small-scale models. In addition, net-to-net wake effects imply a flow velocity reduction in proximity of the rear net of the cage with respect to the frontal one. This reduction depends on S_n , Re and the inflow angle and is usually described by a reduction factor r , such that the force on the rear net is reduced by a factor r^2 . Traditionally [168,169,172], this value is calculated as a function of C_d only: $r = 1 - 0.46C_d$. Consequently, only C_d variability with Re is here considered for scaling purposes. It is worth noting that slight variations of C_d tends to be compensated by opposite variations of r , while larger variations imply significant inaccuracies in physical model representativeness. Cheng et al. [168] review and compare different literature studies for the estimation of C_d , observing that, in general, its variability is low (between 1.1 and 1.3) in the range $100 < Re < 10^4$, including almost all practical offshore aquaculture applications. In this perspective, the maximum scale effect in terms of C_d should weigh about 18%, which becomes about 10% in terms of drag forces, taking into account also the effects of r . It follows that acceptable scaling could be achieved by increasing scaled d_w as much as possible for the given S_n , to keep Re within the mentioned range. This criterion is simple and can be used as a benchmark for scaling activities; however, it derives from a model calibration based mainly on Morison’s approach. To complement it, we suggest to refer to the formulation of Kristiansen and Faltinsen [169], calibrated on a screen model for $S_n \leq 0.5$ and $32 < Re < 10^4$, taking into account large cage deformations and inclined flow angles, and widely used in literature [166,168,170]. In this study, Re was defined by means of Eq. 4, using the undisturbed flow velocity divided

by $(1-S_n)$ as the reference velocity v and the twine diameter d_w as the characteristic length l . Drag and lift coefficients were calculated as a Fourier sum of components:

$$C_D(\theta) = c_d \sum_{n=1}^{\infty} a_{2n-1} \cos[(2n-1)\theta]; \quad C_L(\theta) = c_l \sum_{n=1}^{\infty} b_{2n} \cos(2n\theta), \quad (24)$$

being ϑ the inflow angle, a_i , b_i the Fourier coefficients and c_d , c_l the reference hydrodynamic coefficients. They observed that the Fourier coefficients and the number of contributions necessary for the summations are somehow uncertain but seem to depend only on S_n , hence could be assumed constant after scaling, as long as it is preserved. c_d and c_l , instead, depend on Re , with a set of empiric laws. Fig. 11 shows the estimated reference drag coefficient c_d as a function of Re , for various S_n values. It is worth noting that c_l behavior is analogous, but smaller, hence considering c_d is sufficient for scaling purposes.

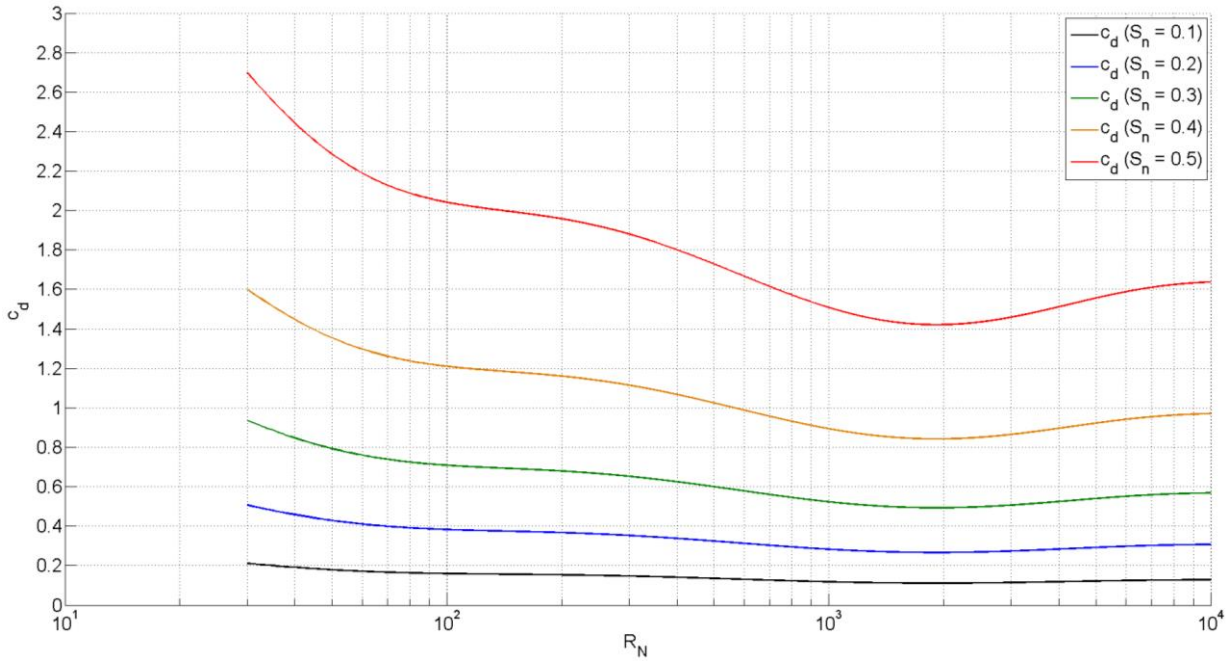


Fig. 11 – Empirical polynomial law for reference drag coefficient c_d , for variable solidity ratios S_n .

It can be observed that the scale effect due to Re reduction predicted by this model may be significant, particularly when scaled Re is very low. In this case, just augmenting the scaled twine diameter may not be the best strategy, particularly if full-scale and small-scale Re ranges attain the ascending and the descending traits of the curve, respectively. If so, d_w should be chosen in a way that the two Re ranges correspond to c_d and c_l coefficients as close as possible between each other. An example of d_w optimization, based on the proposed criterion, can be found in [15], where the arrangement of two 1:40 (indoor) and 1:15 (at-sea) experimental campaign on a MPP were described. In such case, the increase of the model scale from indoor to outdoor testing was crucial to minimize the drag coefficient alteration. In general, full-scale Re ranges are heavily case-dependent, hence each particular case study must be carefully evaluated. In this context, it should be taken into account that fouling may represent a very relevant phenomenon at full scale, since it increases solidity ratio of the cages (hence hydrodynamic forces) and reduces water circulation [173,174]. From a scaling perspective, worst-case scenarios should take into account these effects, by means of opportune modifications of the corresponding cage properties.

The above discussion regards mainly drag forces, which are sufficient to represent the coupling of cages with MPP from the latter point of view. Other phenomena of interest may regard the flexible cage deformation and the corresponding volume reduction, local flow velocities inside and around the cages, etc. These parameters generally have relatively small effects on drag forces [21,166,169], but may be of interest for fish

welfare. However, it is generally not possible to scale net elasticity, as it would require too small Young modules for net materials. Currently, the only feasible option is to estimate them numerically (see e.g. [165,173,175–177]). During experiments, we suggest to keep axial stiffness of the scaled suspension ropes as small as possible. Material and weaving of the twine and the net could affect the turbulence properties, hence the drag forces [178]. It is hence suggested to use the same ones for the model and the prototype. Alternatively, the surface roughness could be purposely modified, to compensate hydrodynamic coefficients alteration due to Re reductions at small-scale (e.g. if the full-scale Re range is already in the descending trait of the curve in Fig. 8). Finally, the scaling of sinker should be based primarily on the wet weight per unit length, and secondly on its bending stiffness, according to Froude laws. These two parameters are indeed important for cage deformation. Sinker diameter and material could be altered, if necessary to meet the bending stiffness requirement, since drag forces on the sinker generally play a secondary role in the overall cage dynamics.

In conclusion, fish net scaling may be important for a MPP physical model, especially in terms of hydrodynamic forces, including nets-induced drag damping. The scaling strategies available are described in this section and summarized schematically in Fig. 12. Given the complexity of the dynamic behavior of such systems, involving very small twines and large local and global deformation, it is always good practice, if possible, to perform dedicated tests on the cage models alone, including towing tests and tests in waves.

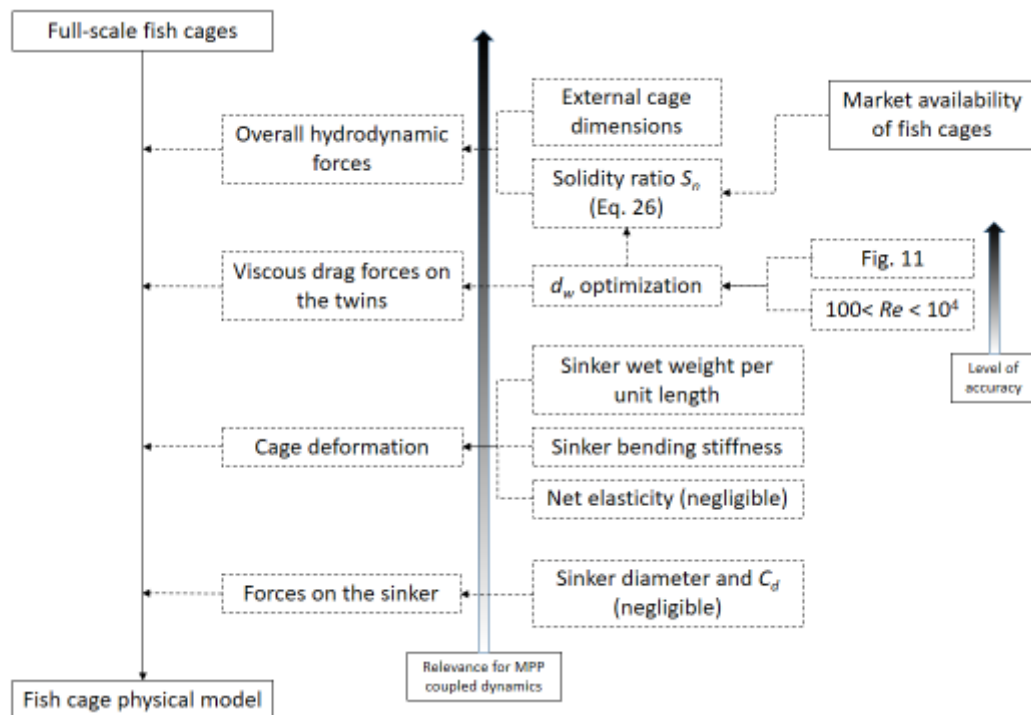


Fig. 12 – Proposed schematic workflow for the design of scaled fish net cages within MPPs.

Although the above information provide some guidance for the scaling of aquaculture cages for MPP physical models, huge research effort is required to deepen the understanding of the cage dynamics and its interaction with integrated floating structures. New dedicated experiments should be carried out to refine the estimation of the hydrodynamic coefficients. In particular, waves and imposed oscillatory motion loads should be investigated in detail, as most of the state-of-the-art literature is based on current loads, while the damping provided by cages in oscillatory flow may be very relevant for MPP dynamics. Finally, numerical studies on cage deformation and flow alteration should be intensified for two main reason: 1) provide reliable assessment of fish welfare, due to the unavoidable scale effects introduced by physical models in terms of net flexibility; 2) clarify their effects on cage-MPP interaction. The latter point is particularly useful in the case of multiple cages, since the wake properties of the front cage may affect the loads on the aft ones.

4. Concluding remarks

Although multi-purpose floating platforms (MPPs) are very attractive for offshore industry, most of the proposed concepts still have very low technology readiness levels, thus they require extensive experimental campaigns before going to an industrial development. In this context, the integration of different subsystems, each with its own physical laws, complicates significantly the design of adequately scaled physical models and the arrangement of the experimental activities. Hence, the present paper proposes a detailed review and discussion about the scaling strategies available for MPPs. Some fundamentals of the scaling theory are illustrated, and application to the specific cases of interest are extensively discussed. In particular, scaling strategies for floating hull, mooring system, wind turbine, oscillating water column (OWC) wave energy converters (WECs) and net cages for aquaculture are considered individually, as they represent the most frequent subsystems proposed for MPPs, and the possible elements of integration between them are presented. Potential test environments for experimental activities are also described, and their advantages and limitations are discussed, with direct applicability to the MPP cases. The considerations collected in the paper may serve as a support for the design choices preparatory to experimental setups, since the interested reader may critically interpret them, in light of the number/kind of sub-systems and the level of detail required by the specific application concerned. Finally, the main uncertainties and criticalities of the state-of-the-art are highlighted and suggestions for future developments, necessary to support scaling activities, are provided.

The key outcomes of the present review study are:

- Froude scaling law, used for floating structure physical modeling, is generally not fully compatible with MPP applications. Indeed, they may introduce significant distortions, e.g. with respect to viscous forces, which are responsible for most of the overall hydrodynamic damping in many practical cases.
- Adequate scaling strategies are proposed for each subsystem, based on STAGE approach, in order to minimize scale effects. The proposed methodology starts from the detailed analysis of the governing equations of the subsystem, aimed to identify its impact on the overall MPP dynamics and adjust scaling accordingly.
- The choice of the scale factor of the physical model governs the range of Reynolds numbers. As the latter is responsible for the estimation of drag coefficients of slender bodies, strategies are proposed to tune the scale factor appropriately, based on the experimental data available from open literature. However, while these data are reliable for slender cylinders, huge uncertainties are detected for even smaller bodies, such as mooring line chains/ropes and fish net twines. Dedicated investigations are hence highly encouraged, to provide opportune support for the design of future experimental activities on MPPs.
- Ideal scaled representation of energy harvesting systems, namely wind turbines and WECs, cannot be achieved by Froude scaling. However, extensive ad-hoc studies have been carried out in literature, leading to several reliable scaling strategies, including real-time hybrid testing, which are introduced in the paper. In this case, great care should be paid also in the selection of the opportune auxiliary numerical models, necessary for their implementation, taking into account the contrasting issues related to the level of detail required and to the computational cost.
- Along with the integration of subsystems with different scaling laws, peculiar criticalities of MPPs, may include large size of the structure, significance of low-frequency effects and elasticity. These may be incompatible with small-scale modeling in indoor wave tanks, which have limitations in size, water depth, wave height, period and direction, and simulation duration.
- Outdoor testing of MPPs at sea in opportune sites may represent a feasible alternative/complement to traditional indoor testing, not only for large-scale prototypal activities but also for intermediate-scale experiments (TRL 5-7). Some advantages would be: scale effects and cost reduction, greater space availability in horizontal and vertical planes, wider range of environmental conditions,

including three-dimensional effects, feasibility of longer tests to investigate low-frequency effects and to perform probabilistic studies.

References

- [1] P. Boccotti, *Wave Mechanics for Ocean Engineering*, Elsevier Oceanography Series, Amsterdam, The Netherlands, 2000.
- [2] W.M. Nassar, O. Anaya-Lara, K.H. Ahmed, D. Campos-Gaona, M. Elgenedy, *Assessment of Multi-Use Offshore Platforms: Structure Classification and Design Challenges*, *Sustainability*. 12 (2020) 1860. <https://doi.org/10.3390/su12051860>.
- [3] C. Pérez-Collazo, D. Greaves, G. Iglesias, *A review of combined wave and offshore wind energy*, *Renew. Sustain. Energy Rev.* 42 (2015) 141–153. <https://doi.org/10.1016/j.rser.2014.09.032>.
- [4] R. Pernice, *Japanese urban artificial islands: an overview of projects and schemes for marine cities during 1960s-1990s*, *J. Archit. Plan. (Transactions AIJ)*. 74 (2009) 1847–1855.
- [5] J.-B. Jouffray, R. Blasiak, A. V. Norström, H. Österblom, M. Nyström, *The Blue Acceleration: The Trajectory of Human Expansion into the Ocean*, *One Earth*. 2 (2020) 43–54. <https://doi.org/https://doi.org/10.1016/j.oneear.2019.12.016>.
- [6] K.A. Abhinav, M. Collu, S. Benjamins, H. Cai, A. Hughes, B. Jiang, S. Jude, W. Leithead, C. Lin, H. Liu, L. Recalde-Camacho, N. Serpetti, K. Sun, B. Wilson, H. Yue, B.-Z. Zhou, *Offshore multi-purpose platforms for a Blue Growth: A technological, environmental and socio-economic review*, *Sci. Total Environ.* 734 (2020) 138256. <https://doi.org/https://doi.org/10.1016/j.scitotenv.2020.138256>.
- [7] M.J. Muliawan, M. Karimirad, T. Moan, *Dynamic response and power performance of a combined Spar-type floating wind turbine and coaxial floating wave energy converter*, *Renew. Energy*. 50 (2013) 47–57. <https://doi.org/https://doi.org/10.1016/j.renene.2012.05.025>.
- [8] C. Michailides, C. Luan, Z. Gao, T. Moan, *Effect of Flap Type Wave Energy Converters on the Response of a Semi-Submersible Wind Turbine in Operational Conditions*, (2014). <https://doi.org/10.1115/OMAE2014-24065>.
- [9] O’Sullivan, Murphy, *Techno-economic optimisation of an oscillating water column array wave energy converter*, in: *Proc. 10th Eur. Wave Tidal Energy Conf. (EWTEC)*, Aalborg, Denmark, 2013: pp. 1–8.
- [10] H2Ocean project, (2015). <http://www.vliz.be/projects/mermaidproject/project/related-projects/h2ocean.html> (accessed May 6, 2020).
- [11] Mermaid project website, (2016). <http://www.vliz.be/projects/mermaidproject/index.html> (accessed May 6, 2020).
- [12] The Blue Growth Farm project website, (2020). <http://www.thebluegrowthfarm.eu/> (accessed May 6, 2020).
- [13] Space@sea project website, (2020). <https://spaceatsea-project.eu/>.
- [14] F. Lagasco, M. Collu, A. Mariotti, E. Safier, F. Arena, T. Atack, G. Brizzi, P. Tett, A. Santoro, S. Bourdier, F. Salcedo Fernandez, S. Muggiasca, I. Larrea, *New Engineering Approach for the Development and Demonstration of a Multi-Purpose Platform for the Blue Growth Economy*, (2019). <https://doi.org/10.1115/OMAE2019-96104>.
- [15] C. Ruzzo, A. Romolo, G. Malara, F. Arena, F. Taruffi, S. Muggiasca, M. Belloli, B. Bouscasse, J. Ohana, A. Santoro, K. Aubriere, G. Brizzi, M. Collu, P. Corvaglia, F. Lagasco, *On the arrangement of two*

experimental activities on a novel multi-purpose floating structure concept, in: Proc. 4th Int. Conf. Renew. Energies Offshore (RENEW2020), Oct. 12-15, Lisbon, Port., 2020.

- [16] M. Flikkema, O. Waals, Space@Sea the Floating Solution, *Front. Mar. Sci.* 6 (2019) 553. <https://doi.org/10.3389/fmars.2019.00553>.
- [17] A. Fontanella, F. Taruffi, S. Muggiasca, M. Belloli, Design Methodology for a Floating Offshore Wind Turbine Large-Scale Outdoor Prototype, (2019). <https://doi.org/10.1115/OMAE2019-95979>.
- [18] S. Muggiasca, A. Fontanella, F. Taruffi, H. Giberti, A. Facchinetti, M. Belloli, M. Bollati, Large Aeroelastic Model of a Floating Offshore Wind Turbine: Mechanical and Mechatronics Design, (2019). <https://doi.org/10.1115/IOWTC2019-7537>.
- [19] A.F.O. Falcão, J.C.C. Henriques, Model-prototype similarity of oscillating-water-column wave energy converters, *Int. J. Mar. Energy.* 6 (2014) 18–34. <https://doi.org/10.1016/j.ijome.2014.05.002>.
- [20] J. Palm, C. Eskilsson, L. Bergdahl, R. Bensow, Assessment of Scale Effects, Viscous Forces and Induced Drag on a Point-Absorbing Wave Energy Converter by CFD Simulations, *J. Mar. Sci. Eng.* 6 (2018) 124. <https://doi.org/10.3390/jmse6040124>.
- [21] A.A. Turner, T.L. Jeans, G.K. Reid, Experimental Investigation of Fish Farm Hydrodynamic Wake Properties on 1:15 Scale Model Circular Aquaculture Cages, in: Proc. 34th Int. Conf. Ocean. Offshore Arct. Eng., 2015: pp. OMAE2015-42140. <https://doi.org/10.1115/OMAE2015-42140>.
- [22] C.M. Wang, Z.Y. Tay, Very Large Floating Structures: Applications, Research and Development, *Procedia Eng.* 14 (2011) 62–72. <https://doi.org/https://doi.org/10.1016/j.proeng.2011.07.007>.
- [23] M. Lamas-Pardo, G. Iglesias, L. Carral, A review of Very Large Floating Structures (VLFS) for coastal and offshore uses, *Ocean Eng.* 109 (2015) 677–690. <https://doi.org/https://doi.org/10.1016/j.oceaneng.2015.09.012>.
- [24] M. Thys, A. Fontanella, F. Taruffi, M. Belloli, P.A. Berthelsen, Hybrid Model Tests for Floating Offshore Wind Turbines, (2019). <https://doi.org/10.1115/IOWTC2019-7575>.
- [25] M. Belloli, I. Bayati, A. Facchinetti, A. Fontanella, H. Giberti, F. La Mura, F. Taruffi, A. Zasso, A hybrid methodology for wind tunnel testing of floating offshore wind turbines, *Ocean Eng.* 210 (2020) 107592. <https://doi.org/https://doi.org/10.1016/j.oceaneng.2020.107592>.
- [26] T. Utsunomiya, H. Matsukuma, S. Minoura, K. Ko, H. Hamamura, O. Kobayashi, I. Sato, Y. Nomoto, K. Yasui, At sea experiment of a hybrid spar for floating offshore wind turbine using 1/10-scale model, *J. Offshore Mech. Arct. Eng.* 135 (2013) 34503–34508. <https://doi.org/10.1115/1.4024148>.
- [27] C. Ruzzo, V. Fiamma, M. Collu, G. Failla, V. Nava, F. Arena, On intermediate-scale open-sea experiments on floating offshore structures: Feasibility and application on a spar support for offshore wind turbines, *Mar. Struct.* 61 (2018) 220–237. <https://doi.org/https://doi.org/10.1016/j.marstruc.2018.06.002>.
- [28] A. Casaburo, G. Petrone, F. Franco, S. De Rosa, A Review of Similitude Methods for Structural Engineering, *Appl. Mech. Rev.* 71 (2019). <https://doi.org/10.1115/1.4043787>.
- [29] C.P. Coutinho, A.J. Baptista, J. Dias Rodrigues, Reduced scale models based on similitude theory: A review up to 2015, *Eng. Struct.* 119 (2016) 81–94. <https://doi.org/https://doi.org/10.1016/j.engstruct.2016.04.016>.
- [30] E. Szucs, *Similitude and modelling*, Elsevier, New York, USA, 1980.
- [31] D. Vassalos, Physical modelling and similitude of marine structures, *Ocean Eng.* 26 (1998) 111–123. [https://doi.org/https://doi.org/10.1016/S0029-8018\(97\)10004-X](https://doi.org/https://doi.org/10.1016/S0029-8018(97)10004-X).
- [32] S.G. Sterrett, Similarity and Dimensional Analysis, in: A.B.T.-P. of T. and E.S. Meijers (Ed.), *Handb.*

Philos. Sci., North-Holland, Amsterdam, 2009: pp. 799–823.
<https://doi.org/https://doi.org/10.1016/B978-0-444-51667-1.50033-1>.

- [33] S. Kaneko, T. Nakamura, F. Inada, M. Kato, K. Ishihara, T. Nishihara, M.A.B.T.-F.V. (Second E. Langthjem, eds., Chapter 2 - Vibration Induced by Cross-Flow, in: Academic Press, Oxford, 2014: pp. 29–115. <https://doi.org/https://doi.org/10.1016/B978-0-08-098347-9.00002-3>.
- [34] Kelvin Hydrodynamic Laboratory, (n.d.).
<https://www.strath.ac.uk/engineering/navalarchitectureoceanmarineengineering/ourfacilities/kelvinhydrodynamiclaboratory/>.
- [35] State Key Laboratory of Ocean Engineering, Deepwater Offshore Basin, (n.d.).
<http://oe.sjtu.edu.cn/EN/list.php?id=26&t=3>.
- [36] ITTC, Resistance Test, (2017) Procedure 7.5-02-02-01, Pag. 1-14.
- [37] ITTC, Active Hybrid Model Tests of Floating Offshore Structures with Mooring Lines, (2017) Procedure 7.5-02-07-03.4.
- [38] ITTC, Passive Hybrid Model Tests of Floating Offshore Structures with Mooring Lines, (2017) Procedure 7.5-02-07-03.4.
- [39] L. Wan, Z. Gao, T. Moan, C. Lugni, Experimental and numerical comparisons of hydrodynamic responses for a combined wind and wave energy converter concept under operational conditions, *Renew. Energy*. 93 (2016) 87–100. <https://doi.org/https://doi.org/10.1016/j.renene.2016.01.087>.
- [40] S.K. Chakrabarti, Chapter 13 - Physical Modelling of Offshore Structures, in: S.K.B.T.-H. of O.E. CHAKRABARTI (Ed.), Elsevier, London, 2005: pp. 1001–1054.
<https://doi.org/https://doi.org/10.1016/B978-0-08-044381-2.50020-5>.
- [41] Hidrodynamic and ocean engineering tank - Ecole Centrale de Nantes facilities, (n.d.).
<https://lheea.ec-nantes.fr/test-facilities/ocean-tanks/hydrodynamic-and-ocean-engineering-tank>.
- [42] Wave flume facilities - HR Wallingford, (n.d.). <https://www.hrwallingford.com/facilities/wave-flumes>.
- [43] I. Bayati, A. Facchinetti, A. Fontanella, H. Giberti, M. Belloli, A wind tunnel/HIL setup for integrated tests of Floating Offshore Wind Turbines, *J. Phys. Conf. Ser.* 1037 (2018).
<https://doi.org/10.1088/1742-6596/1037/5/052025>.
- [44] A. Fontanella, I. Bayati, F. Taruffi, A. Facchinetti, M. Belloli, Numerical and Experimental Wind Tunnel Analysis of Aerodynamic Effects on a Semi-Submersible Floating Wind Turbine Response, (2019).
<https://doi.org/10.1115/OMAE2019-95976>.
- [45] I. Bayati, A. Facchinetti, A. Fontanella, F. Taruffi, M. Belloli, Analysis of FOWT dynamics in 2-DOF hybrid HIL wind tunnel experiments, *Ocean Eng.* 195 (2020) 106717.
<https://doi.org/https://doi.org/10.1016/j.oceaneng.2019.106717>.
- [46] GVPM - Wind Tunnel Politecnico di Milano, (n.d.). <http://www.windtunnel.polimi.it/>.
- [47] S. Ishida, K. Kokubun, T. Nimura, T. Utsunomiya, I. Sato, S. Yoshida, At-Sea Experiment of a Hybrid SPAR Type Offshore Wind Turbine, (2013). <https://doi.org/10.1115/OMAE2013-10655>.
- [48] A.M. Viselli, A.J. Goupee, H.J. Dagher, Model Test of a 1:8-Scale Floating Wind Turbine Offshore in the Gulf of Maine¹, *J. Offshore Mech. Arct. Eng.* 137 (2015). <https://doi.org/10.1115/1.4030381>.
- [49] T. Utsunomiya, H. Matsukuma, S. Minoura, K. Ko, H. Hamamura, O. Kobayashi, I. Sato, Y. Nomoto, K. Yasui, On Sea Experiment of a Hybrid SPAR for Floating Offshore Wind Turbine Using 1/10 Scale Model, (2010) 529–536. <https://doi.org/10.1115/OMAE2010-20730>.

- [50] C. Ruzzo, N. Saha, F. Arena, Wave spectral analysis for design of a spar floating wind turbine in Mediterranean Sea, *Ocean Eng.* 184 (2019) 255–272. <https://doi.org/https://doi.org/10.1016/j.oceaneng.2019.05.027>.
- [51] C. Ruzzo, G. Failla, M. Collu, V. Nava, V. Fiamma, F. Arena, Operational modal analysis of a spar-type floating platform using frequency domain decomposition method, *Energies*. 9 (2016). <https://doi.org/10.3390/en9110870>.
- [52] C. Ruzzo, G. Failla, M. Collu, V. Nava, V. Fiamma, F. Arena, Output-only identification of rigid body motions of floating structures: A case study, in: *Procedia Eng.*, Elsevier Ltd, 2017: pp. 930–935. <https://doi.org/10.1016/j.proeng.2017.09.243>.
- [53] F. Pimenta, C. Ruzzo, G. Failla, F. Arena, M. Alves, F. Magalhães, Dynamic Response Characterization of Floating Structures Based on Numerical Simulations, *Energies* 2020, Vol. 13, Page 5670. 13 (2020) 5670. <https://doi.org/10.3390/EN13215670>.
- [54] P. Boccotti, *Wave Mechanics and Wave Loads on Marine Structures*, Butterworth-Heinemann (Elsevier), Oxford, 2014. <https://doi.org/10.1016/C2013-0-13663-X>.
- [55] Natural Ocean Engineering Laboratory (NOEL), (2020). <http://noel.unirc.it/> (accessed May 18, 2020).
- [56] F. Arena, G. Barbaro, The Natural Ocean Engineering Laboratory, NOEL, in Reggio Calabria, Italy: A Commentary and Announcement, *J. Coast. Res.* 290 (2013) vii–x. <https://doi.org/10.2112/13A-00004>.
- [57] O.M. Faltinsen, *Sea loads on ships and offshore structures*, Cambridge University Press, Cambridge, UK, 1990.
- [58] Z. Gao, T. Moan, L. Wan, C. Michailides, Comparative numerical and experimental study of two combined wind and wave energy concepts, *J. Ocean Eng. Sci.* 1 (2016) 36–51. <https://doi.org/https://doi.org/10.1016/j.joes.2015.12.006>.
- [59] J.R. Morison, J.W. Johnson, S.A. Schaaf, The Force Exerted by Surface Waves on Piles, *J. Pet. Technol.* 2 (1950) 149–154. <https://doi.org/10.2118/950149-G>.
- [60] L.E. Borgman, Computation of the ocean-wave forces on inclined cylinders, *Eos, Trans. Am. Geophys. Union.* 39 (1958) 885–888. <https://doi.org/10.1029/TR039i005p00885>.
- [61] T. Sarpkaya, M. Isaacson, *Mechanics of wave forces on offshore structures.*, (1981). [https://doi.org/10.1016/0261-7277\(82\)90028-6](https://doi.org/10.1016/0261-7277(82)90028-6).
- [62] P. Boccotti, F. Arena, V. Fiamma, G. Barbaro, Field experiment on random wave forces acting on vertical cylinders, *Probabilistic Eng. Mech.* 28 (2012) 39–51. <https://doi.org/https://doi.org/10.1016/j.probengmech.2011.08.003>.
- [63] P. Boccotti, F. Arena, V. Fiamma, A. Romolo, Two small-scale field experiments on the effectiveness of Morison’s equation, *Ocean Eng.* 57 (2013) 141–149. <https://doi.org/10.1016/j.oceaneng.2012.08.011>.
- [64] M.E. McCormick, *Ocean Engineering Mechanics: With Applications*, Cambridge University Press, Cambridge, UK, 2010.
- [65] DNV, *DNV Recommended Practice DNV-RP-C205.*, Det Norske Veritas, Norway, 2010.
- [66] R. van ’t Veer, A. Pistidda, A. Koop, Forces On Bilge Keels In Regular And Irregular Oscillating Flow, *Twenty-Second Int. Offshore Polar Eng. Conf.* (2012) 8. <https://doi.org/>.
- [67] J. Fitzgerald, L. Bergdahl, Rigid moorings in shallow water: A wave power application. Part I: Experimental verification of methods, *Mar. Struct.* 22 (2009) 809–835. <https://doi.org/https://doi.org/10.1016/j.marstruc.2009.09.002>.

- [68] J. Jonkman, Definition of the Floating System for Phase IV of OC3, 2010. <http://www.osti.gov/bridge> (accessed May 7, 2020).
- [69] A.J. Goupee, B. Koo, K. Lambrakos, R. Kimball, Model Tests for Three Floating Wind Turbine Concepts, *Offshore Technol. Conf.* (2012) 16. <https://doi.org/10.4043/23470-MS>.
- [70] H. Shin, P.T. Dam, K.J. Jung, J. Song, C. Rim, T. Chung, Model test of new floating offshore wind turbine platforms, *Int. J. Nav. Archit. Ocean Eng.* 5 (2013) 199–209. <https://doi.org/https://doi.org/10.2478/IJNAOE-2013-0127>.
- [71] S. Hong, I. Lee, S.H. Park, C. Lee, H.-H. Chun, H.C. Lim, An experimental study of the effect of mooring systems on the dynamics of a SPAR buoy-type floating offshore wind turbine, *Int. J. Nav. Archit. Ocean Eng.* 7 (2015) 559–579. <https://doi.org/https://doi.org/10.1515/ijnaoe-2015-0040>.
- [72] F. Duan, Z. Hu, J.M. Niedzwecki, Model test investigation of a spar floating wind turbine, *Mar. Struct.* 49 (2016) 76–96. <https://doi.org/https://doi.org/10.1016/j.marstruc.2016.05.011>.
- [73] C. Ng, R. Jiang, Classification Principles for Very Large Floating Structures BT - WCFS2019, in: C.M. Wang, S.H. Lim, Z.Y. Tay (Eds.), Springer Singapore, Singapore, 2020: pp. 235–251.
- [74] S. Ohmatsu, Model experiments for VLFS, in: C.M. Wang, E. Watanabe, T. Utsunomiya (Eds.), *Very Large Float. Struct.*, Taylor & Francis, 2008: pp. 141–164.
- [75] P. Yang, X. Liu, Z. Wang, Z. Zong, C. Tian, Y. Wu, Hydroelastic responses of a 3-module VLFS in the waves influenced by complicated geographic environment, *Ocean Eng.* 184 (2019) 121–133. <https://doi.org/https://doi.org/10.1016/j.oceaneng.2019.05.020>.
- [76] H. Suzuki, H.R. Riggs, M. Fujikubo, T.A. Shugar, H. Seto, Y. Yasuzawa, B. Bhattacharya, D.A. Hudson, H. Shin, *Very Large Floating Structures*, (2007) 597–608. <https://doi.org/10.1115/OMAE2007-29758>.
- [77] Y. Cheng, C. Ji, G. Zhai, G. Oleg, Fully nonlinear numerical investigation on hydroelastic responses of floating elastic plate over variable depth sea-bottom, *Mar. Struct.* 55 (2017) 37–61. <https://doi.org/https://doi.org/10.1016/j.marstruc.2017.04.005>.
- [78] J. Ding, C. Tian, Y. Wu, Z. Li, H. Ling, X. Ma, Hydroelastic analysis and model tests of a single module VLFS deployed near islands and reefs, *Ocean Eng.* 144 (2017) 224–234. <https://doi.org/https://doi.org/10.1016/j.oceaneng.2017.08.043>.
- [79] J.-G. Kim, S.-P. Cho, K.-T. Kim, P.-S. Lee, Hydroelastic design contour for the preliminary design of very large floating structures, *Ocean Eng.* 78 (2014) 112–123. <https://doi.org/https://doi.org/10.1016/j.oceaneng.2013.11.006>.
- [80] A.E. Karperaki, K.A. Belibassakis, T.K. Papathanasiou, Time-domain, shallow-water hydroelastic analysis of VLFS elastically connected to the seabed, *Mar. Struct.* 48 (2016) 33–51. <https://doi.org/https://doi.org/10.1016/j.marstruc.2016.04.002>.
- [81] D. Wang, R.C. Ertekin, H.R. Riggs, Three-Dimensional Hydroelastic Response Of A Very Large Floating Structure, *Int. J. Offshore Polar Eng.* 1 (1991) 10. <https://doi.org/>.
- [82] H.R. Riggs, R.C. Ertekin, T.R.J. Mills, A comparative study of RMFC and FEA models for the wave-induced response of a MOB, *Mar. Struct.* 13 (2000) 217–232. [https://doi.org/https://doi.org/10.1016/S0951-8339\(00\)00029-0](https://doi.org/https://doi.org/10.1016/S0951-8339(00)00029-0).
- [83] H. Zhang, D. Xu, S. Xia, G. Shi, R. Ding, Dynamics of super-scale modularized floating airport, in: C.M. Wang, S.H. Lim, Z.Y. Tay (Eds.), *Proc. World Conf. Float. Solut.*, Springer Singapore, 2019. https://doi.org/https://doi.org/10.1007/978-981-13-8743-2_6.
- [84] P. Yang, Z. Li, Y. Wu, W. Wen, J. Ding, Z. Zhang, Boussinesq-Hydroelasticity coupled model to investigate hydroelastic responses and connector loads of an eight-module VLFS near islands in time

domain, *Ocean Eng.* 190 (2019) 106418.

<https://doi.org/https://doi.org/10.1016/j.oceaneng.2019.106418>.

- [85] J. Ding, Y. Wu, Y. Zhou, X.-Z. Ma, H.J. Ling, Z. Xie, Investigation of connector loads of a 3-module VLFS using experimental and numerical methods, *Ocean Eng.* 195 (2020) 106684.
<https://doi.org/https://doi.org/10.1016/j.oceaneng.2019.106684>.
- [86] L. Martinelli, B. Zanuttigh, Effects of Mooring Compliancy on the Mooring Forces, Power Production, and Dynamics of a Floating Wave Activated Body Energy Converter, *Energies*. 11 (2018) 3535.
<https://doi.org/10.3390/en11123535>.
- [87] J.F. Luxmoore, S. Grey, D. Newsam, L. Johanning, Analytical performance assessment of a novel active mooring system for load reduction in marine energy converters, *Ocean Eng.* 124 (2016) 215–225. <https://doi.org/https://doi.org/10.1016/j.oceaneng.2016.07.047>.
- [88] J. Davidson, J. V. Ringwood, Mathematical Modelling of Mooring Systems for Wave Energy Converters—A Review, *Energies*. 10 (2017) 666. <https://doi.org/10.3390/en10050666>.
- [89] S. Xu, S. Wang, C. Guedes Soares, Review of mooring design for floating wave energy converters, *Renew. Sustain. Energy Rev.* 111 (2019) 595–621.
<https://doi.org/https://doi.org/10.1016/j.rser.2019.05.027>.
- [90] C. Barrera, R. Guanche, Á. Rodríguez, J.A. Armesto, I.J. Losada, On the importance of mooring system parametrisation for accurate floating structure designs, *Mar. Struct.* 72 (2020) 102765.
<https://doi.org/https://doi.org/10.1016/j.marstruct.2020.102765>.
- [91] L. Johanning, G.H. Smith, J. Wolfram, Measurements of static and dynamic mooring line damping and their importance for floating WEC devices, *Ocean Eng.* 34 (2007) 1918–1934.
<https://doi.org/https://doi.org/10.1016/j.oceaneng.2007.04.002>.
- [92] C. Barrera, R. Guanche, I.J. Losada, Experimental modelling of mooring systems for floating marine energy concepts, *Mar. Struct.* 63 (2019) 153–180.
<https://doi.org/https://doi.org/10.1016/j.marstruct.2018.08.003>.
- [93] I. Touzon, B. de Miguel, V. Nava, V. Petuya, I. Mendikoa, F. Boscolo, Mooring System Design Approach: A Case Study for MARMOK-A Floating OWC Wave Energy Converter, (2018).
<https://doi.org/10.1115/OMAE2018-77634>.
- [94] P. Trubat, C. Molins, X. Gironella, Wave hydrodynamic forces over mooring lines on floating offshore wind turbines, *Ocean Eng.* 195 (2020) 106730.
<https://doi.org/https://doi.org/10.1016/j.oceaneng.2019.106730>.
- [95] P.K. Stansby, E. Carpintero Moreno, D.D. Apsley, T.J. Stallard, Slack-moored semi-submersible wind floater with damping plates in waves: Linear diffraction modelling with mean forces and experiments, *J. Fluids Struct.* 90 (2019) 410–431.
<https://doi.org/https://doi.org/10.1016/j.jfluidstructs.2019.07.010>.
- [96] M. Hall, A. Goupee, Validation of a lumped-mass mooring line model with DeepCwind semisubmersible model test data, *Ocean Eng.* 104 (2015) 590–603.
<https://doi.org/https://doi.org/10.1016/j.oceaneng.2015.05.035>.
- [97] I. Touzon, V. Nava, Z. Gao, I. Mendikoa, V. Petuya, Small scale experimental validation of a numerical model of the HarshLab2.0 floating platform coupled with a non-linear lumped mass catenary mooring system, *Ocean Eng.* 200 (2020) 107036.
<https://doi.org/https://doi.org/10.1016/j.oceaneng.2020.107036>.
- [98] J. Fitzgerald, L. Bergdahl, Including moorings in the assessment of a generic offshore wave energy converter: A frequency domain approach, *Mar. Struct.* 21 (2008) 23–46.

<https://doi.org/https://doi.org/10.1016/j.marstruc.2007.09.004>.

- [99] S. Xu, C. Ji, C. Guedes Soares, Experimental study on taut and hybrid moorings damping and their relation with system dynamics, *Ocean Eng.* 154 (2018) 322–340. <https://doi.org/https://doi.org/10.1016/j.oceaneng.2018.01.085>.
- [100] R.M. Raaijmakers, *The influence of Mooring Lines on the Damping of Low Frequency Motions of Moored Offshore Structures*, TUDelft, 1995.
- [101] D.T. Brown, S. Mavrakos, Comparative study on mooring line dynamic loading, *Mar. Struct.* 12 (1999) 131–151. [https://doi.org/https://doi.org/10.1016/S0951-8339\(99\)00011-8](https://doi.org/https://doi.org/10.1016/S0951-8339(99)00011-8).
- [102] X. Chen, J. Zhang, W. Ma, On dynamic coupling effects between a spar and its mooring lines, *Ocean Eng.* 28 (2001) 863–887. [https://doi.org/https://doi.org/10.1016/S0029-8018\(00\)00026-3](https://doi.org/https://doi.org/10.1016/S0029-8018(00)00026-3).
- [103] S.A. Mavrakos, V.J. Papazoglou, M.S. Triantafyllou, J. Hatjigeorgiou, Deep water mooring dynamics, *Mar. Struct.* 9 (1996) 181–209. [https://doi.org/https://doi.org/10.1016/0951-8339\(94\)00019-0](https://doi.org/https://doi.org/10.1016/0951-8339(94)00019-0).
- [104] B.W. Kim, H.G. Sung, J.H. Kim, S.Y. Hong, Comparison of linear spring and nonlinear FEM methods in dynamic coupled analysis of floating structure and mooring system, *J. Fluids Struct.* 42 (2013) 205–227. <https://doi.org/https://doi.org/10.1016/j.jfluidstructs.2013.07.002>.
- [105] Z. Xu, S. Huang, Numerical investigation of mooring line damping and the drag coefficients of studless chain links, *J. Mar. Sci. Appl.* 13 (2014) 76–84. <https://doi.org/10.1007/s11804-014-1235-0>.
- [106] E. Huse, *New Developments in Prediction of Mooring System Damping*, *Offshore Technol. Conf.* (1991) 8. <https://doi.org/10.4043/6593-MS>.
- [107] C. Høeg, Z. Zhang, The influence of different mooring line models on the stochastic dynamic responses of floating wind turbines, *J. Phys. Conf. Ser.* 1037 (2018) 062016. <https://doi.org/10.1088/1742-6596/1037/6/062016>.
- [108] L. Bergdahl, J. Palm, C. Eskilsson, J. Lindahl, Dynamically Scaled Model Experiment of a Mooring Cable, *J. Mar. Sci. Eng.* 4 (2016) 5. <https://doi.org/10.3390/jmse4010005>.
- [109] S.A. Hughes, *Physical Models and Laboratory Techniques in Coastal Engineering*, World Scientific, 1993. <https://doi.org/10.1142/9789812795939>.
- [110] V. Nava, J. Galván, M. Sánchez-Lara, C. Garrido-Mendoza, G. Pérez-Moràn, M. Le Bolluec, B. Augier, R. Rodriguez-Arias, Hydrodynamic identification of NAUTILUS FOWT platform from small scale tests, in: C. Guedes Soares (Ed.), *Adv. Renew. Energies Offshore Proc. 3rd Int. Conf. Renew. Energies Offshore (RENEW2018)*, Oct. 8-10, 2018, Lisbon, Port., Taylor & Francis Group, London, UK, 2019.
- [111] J.E. Gutiérrez-Romero, J. García-Espinosa, B. Serván-Camas, B. Zamora-Parra, Non-linear dynamic analysis of the response of moored floating structures, *Mar. Struct.* 49 (2016) 116–137. <https://doi.org/https://doi.org/10.1016/j.marstruc.2016.05.002>.
- [112] V.J. Papazoglou, S.A. Mavrakos, M.S. Triantafyllou, Non-linear cable response and model testing in water, *J. Sound Vib.* 140 (1990) 103–115. [https://doi.org/https://doi.org/10.1016/0022-460X\(90\)90909-J](https://doi.org/https://doi.org/10.1016/0022-460X(90)90909-J).
- [113] W. C. Webster, Mooring-induced damping, *Ocean Eng.* 22 (1995) 571–591. [https://doi.org/https://doi.org/10.1016/0029-8018\(94\)00027-5](https://doi.org/https://doi.org/10.1016/0029-8018(94)00027-5).
- [114] J. Withers, A. Dercksen, Investigation Into Scale Effects On Motions And Mooring Forces Of A Turret-Moored Tanker, *Offshore Technol. Conf.* (1994) 14. <https://doi.org/10.4043/7444-MS>.
- [115] W.S. Yang, *Hydrodynamic analysis of mooring lines based on optical tracking experiments*, Texas A&M University, 2007.

- [116] DNV GL, DNVGL-RP-F205: Global Performance Analysis of Deepwater Floating Structures, (2017).
- [117] DNV GL, DNVGL-OS-E301 Position mooring, (2015).
- [118] G.J. Lyons, D.T. Brown, H.M. Lin, Drag Coefficients For Mooring Line Hydrodynamic Damping, Seventh Int. Offshore Polar Eng. Conf. (1997) 7. <https://doi.org/>.
- [119] O.J. Waals, R.R.T. van Dijk, Truncation Methods for Deep Water Mooring Systems for a catenary moored FPSO and a Semi Taut Moored Semi Submersible, in: Deep Offshore Technol. Int. Conf., Houston, Texas, USA, 2004.
- [120] H. Wang, G. Ma, L. Sun, Z. Kang, Truncation Design and Model Testing of a Deepwater FPSO Mooring System, J. Offshore Mech. Arct. Eng. 138 (2016). <https://doi.org/10.1115/1.4032605>.
- [121] C. Molins, P. Trubat, X. Gironella, A. Campos, Design Optimization for a Truncated Catenary Mooring System for Scale Model Test, J. Mar. Sci. Eng. 3 (2015) 1362–1381. <https://doi.org/10.3390/jmse3041362>.
- [122] D. Qiao, J.P. Ou, Truncated model tests for mooring lines of a semi-submersible platform and its equivalent compensated method, J. Mar. Sci. Technol. 22 (2014) 125–136. <https://doi.org/10.6119/JMST-013-0108-1>.
- [123] A.P. Argyros, R.S. Langley, R. V Ahilan, Simplifying Mooring Analysis For Deepwater Systems Using Truncation, in: Proc. 21th Int. Offshore Polar Eng. Conf., International Society of Offshore and Polar Engineers, 2011.
- [124] C. Ji, S. Xu, Verification of a hybrid model test method for a deep water floating system with large truncation factor, Ocean Eng. 92 (2014) 245–254. <https://doi.org/https://doi.org/10.1016/j.oceaneng.2014.09.047>.
- [125] S.A. Vilsen, T. Sauder, A.J. Sørensen, M. Føre, Method for Real-Time Hybrid Model Testing of ocean structures: Case study on horizontal mooring systems, Ocean Eng. 172 (2019) 46–58. <https://doi.org/https://doi.org/10.1016/j.oceaneng.2018.10.042>.
- [126] T. Fan, N. Ren, Y. Cheng, C. Chen, J. Ou, Applicability analysis of truncated mooring system based on static and damping equivalence, Ocean Eng. 147 (2018) 458–475. <https://doi.org/https://doi.org/10.1016/j.oceaneng.2017.10.033>.
- [127] EU, EN 1991-1-4: Eurocode 1: Actions on structures - Part 1-4: General actions - Wind actions, (2010). <https://www.phd.eng.br/wp-content/uploads/2015/12/en.1991.1.4.2005.pdf>.
- [128] H. Bredmose, R. Mikkelsen, M. Hansen, R. Laugesen, N. Heilskov, B. Jensen, J. Kirkegaard, Experimental study of the DTU 10 MW wind turbine on a TLP floater in waves and wind, in: Proc. EWEA 2015- Int. Wind Energy Conf., Copenhagen, Denmark, 2015.
- [129] I. Bayati, M. Belloli, L. Bernini, A. Zasso, Aerodynamic design methodology for wind tunnel tests of wind turbine rotors, J. Wind Eng. Ind. Aerodyn. 167 (2017) 217–227. <https://doi.org/https://doi.org/10.1016/j.jweia.2017.05.004>.
- [130] J.M. Jonkman, M.L. Buhl, FAST User's Guide, 2005. <https://www.nrel.gov/docs/fy06osti/38230.pdf>.
- [131] T. Chujo, S. Ishida, Y. Minami, T. Nimura, S. Inoue, Model Experiments on the Motion of a SPAR Type Floating Wind Turbine in Wind and Waves, (2011) 655–662. <https://doi.org/10.1115/OMAE2011-49793>.
- [132] C. Cermelli, D. Roddier, A. Aubault, WindFloat: A Floating Foundation for Offshore Wind Turbines— Part II: Hydrodynamics Analysis, (2009) 135–143. <https://doi.org/10.1115/OMAE2009-79231>.
- [133] M. Kraskowski, K. Zawadzki, A. Rylke, A Method for Computational and Experimental Analysis of the Moored Wind Turbine Seakeeping, in: Present. 18th Australas. Fluid Mech. Conf., Launceston,

Australia, 2012.

- [134] A.J. Goupee, B. Koo, R.W. Kimball, K.F. Lambrakos, H.J. Dagher, Experimental Comparison of Three Floating Wind Turbine Concepts, (2012) 467–476. <https://doi.org/10.1115/OMAE2012-83645>.
- [135] H. Shin, B. Kim, P.T. Dam, K. Jung, Motion of OC4 5MW Semi-Submersible Offshore Wind Turbine in Irregular Waves, (2013). <https://doi.org/10.1115/OMAE2013-10463>.
- [136] B. Wen, X. Tian, X. Dong, Z. Li, Z. Peng, W. Zhang, K. Wei, Design approaches of performance-scaled rotor for wave basin model tests of floating wind turbines, *Renew. Energy*. 148 (2020) 573–584. <https://doi.org/https://doi.org/10.1016/j.renene.2019.10.147>.
- [137] L. Li, Y. Gao, Z. Hu, Z. Yuan, S. Day, H. Li, Model test research of a semisubmersible floating wind turbine with an improved deficient thrust force correction approach, *Renew. Energy*. 119 (2018) 95–105. <https://doi.org/https://doi.org/10.1016/j.renene.2017.12.019>.
- [138] E.E. Bachynski, V. Chabaud, T. Sauder, Real-time Hybrid Model Testing of Floating Wind Turbines: Sensitivity to Limited Actuation, *Energy Procedia*. 80 (2015) 2–12. <https://doi.org/https://doi.org/10.1016/j.egypro.2015.11.400>.
- [139] J. Azcona, H. Bredmose, F. Campagnolo, R. Pereira, F. Sandner, Methods for performing scale-tests for method and model validation of floating wind turbines, (2014).
- [140] L. Li, M. Collu, Y. Gao, C. Ruzzo, F. Arena, F. Taruffi, S. Muggiasca, M. Belloli, Development and validation of a coupled numerical model for offshore floating multi-purpose platforms., in: *Proc. 4th Int. Conf. Renew. Energies Offshore*, Lisbon, Portugal, 2020.
- [141] T. Sauder, V. Chabaud, M. Thys, E.E. Bachynski, L.O. Sæther, Real-Time Hybrid Model Testing of a Braceless Semi-Submersible Wind Turbine: Part I — The Hybrid Approach, in: *Proc. 35th Int. Conf. Ocean. Offshore Arct. Eng.*, 2016: pp. OMAE2016-54435. <https://doi.org/https://doi.org/10.1115/OMAE2016-54435>.
- [142] E.E. Bachynski, M. Thys, T. Sauder, V. Chabaud, L.O. Sæther, Real-Time Hybrid Model Testing of a Braceless Semi-Submersible Wind Turbine: Part II — Experimental Results, in: *Proc. 35th Int. Conf. Ocean. Offshore Arct. Eng.*, Busan, Korea, 2016: pp. OMAE2016-54437. <https://doi.org/https://doi.org/10.1115/OMAE2016-54437>.
- [143] IEC 61400-2, Wind turbines - Part 2: design requirements for small wind turbines, (2006).
- [144] H.P. Nguyen, C.M. Wang, F. Flocard, D.M. Pedroso, Extracting energy while reducing hydroelastic responses of VLFS using a modular raft wec-type attachment, *Appl. Ocean Res.* 84 (2019) 302–316. <https://doi.org/https://doi.org/10.1016/j.apor.2018.11.016>.
- [145] A.F. de O. Falcão, Wave energy utilization: A review of the technologies, *Renew. Sustain. Energy Rev.* 14 (2010) 899–918. <https://doi.org/10.1016/j.rser.2009.11.003>.
- [146] P. Boccotti, Caisson breakwaters embodying an OWC with a small opening—Part I: Theory, *Ocean Eng.* 34 (2007) 806–819. <https://doi.org/10.1016/J.OCEANENG.2006.04.006>.
- [147] G. Ibarra-Berastegi, J. Sáenz, A. Ulazia, P. Serras, G. Esnaola, C. Garcia-Soto, Electricity production, capacity factor, and plant efficiency index at the Mutriku wave farm (2014–2016), *Ocean Eng.* 147 (2018) 20–29. <https://doi.org/10.1016/j.oceaneng.2017.10.018>.
- [148] D.C. Hong, S.Y. Hong, S.W. Hong, Reduction of hydroelastic responses of a very-long floating structure by a floating oscillating-water-column breakwater system, *Ocean Eng.* 33 (2006) 610–634. <https://doi.org/https://doi.org/10.1016/j.oceaneng.2005.06.005>.
- [149] D. Howe, J.-R. Nader, G. Macfarlane, Performance analysis of a floating breakwater integrated with multiple oscillating water column wave energy converters in regular and irregular seas, *Appl. Ocean*

Res. 99 (2020) 102147. <https://doi.org/https://doi.org/10.1016/j.apor.2020.102147>.

- [150] D. Howe, J.-R. Nader, G. Macfarlane, Experimental investigation of multiple Oscillating Water Column Wave Energy Converters integrated in a floating breakwater: Energy extraction performance, *Appl. Ocean Res.* 97 (2020) 102086. <https://doi.org/https://doi.org/10.1016/j.apor.2020.102086>.
- [151] A.F.O. Falcão, J.C.C. Henriques, The spring-like air compressibility effect in oscillating-water-column wave energy converters: Review and analyses, *Renew. Sustain. Energy Rev.* 112 (2019) 483–498. <https://doi.org/10.1016/J.RSER.2019.04.040>.
- [152] A.J.N.A. Sarmiento, Model-Test Optimization Of An Owc Wave Power Plant, *Int. J. Offshore Polar Eng.* 3 (1993) 7. <https://doi.org/>.
- [153] P. Benreguig, M. Vicente, A. Dunne, J. Murphy, Modelling Approaches of a Closed-Circuit OWC Wave Energy Converter, *J. Mar. Sci. Eng.* 7 (2019) 23. <https://doi.org/10.3390/jmse7020023>.
- [154] A.F.O. Falcão, J.C.C. Henriques, Oscillating-water-column wave energy converters and air turbines: A review, *Renew. Energy.* 85 (2016) 1391–1424. <https://doi.org/10.1016/j.renene.2015.07.086>.
- [155] G. Moretti, G. Malara, A. Scialò, L. Daniele, A. Romolo, R. Vertechy, M. Fontana, F. Arena, Modelling and field testing of a breakwater-integrated U-OWC wave energy converter with dielectric elastomer generator, *Renew. Energy.* 146 (2020) 628–642. <https://doi.org/10.1016/J.RENENE.2019.06.077>.
- [156] P. Boccotti, P. Filianoti, V. Fiamma, F. Arena, Caisson breakwaters embodying an OWC with a small opening-Part II: A small-scale field experiment, *Ocean Eng.* 34 (2007) 820–841. <https://doi.org/10.1016/j.oceaneng.2006.04.016>.
- [157] A. Viviano, S. Naty, E. Foti, T. Bruce, W. Allsop, D. Vicinanza, Large-scale experiments on the behaviour of a generalised Oscillating Water Column under random waves, *Renew. Energy.* 99 (2016) 875–887. <https://doi.org/https://doi.org/10.1016/j.renene.2016.07.067>.
- [158] R.P.F. Gomes, J.C.C. Henriques, L.M.C. Gato, A.F.O. Falcão, Time-domain simulation of a slack-moored floating oscillating water column and validation with physical model tests, *Renew. Energy.* 149 (2020) 165–180. <https://doi.org/https://doi.org/10.1016/j.renene.2019.11.159>.
- [159] A. Elhanafi, G. Macfarlane, A. Fleming, Z. Leong, Experimental and numerical investigations on the hydrodynamic performance of a floating–moored oscillating water column wave energy converter, *Appl. Energy.* 205 (2017) 369–390. <https://doi.org/https://doi.org/10.1016/j.apenergy.2017.07.138>.
- [160] U. Singh, N. Abdussamie, J. Hore, Hydrodynamic performance of a floating offshore OWC wave energy converter: An experimental study, *Renew. Sustain. Energy Rev.* 117 (2020) 109501. <https://doi.org/https://doi.org/10.1016/j.rser.2019.109501>.
- [161] J. Sarmiento, A. Iturrioz, V. Ayllón, R. Guanache, I.J. Losada, Experimental modelling of a multi-use floating platform for wave and wind energy harvesting, *Ocean Eng.* 173 (2019) 761–773. <https://doi.org/https://doi.org/10.1016/j.oceaneng.2018.12.046>.
- [162] J.E. Huguenin, F.J. Ansuini, A review of the technology and economics of marine fish cage systems, *Aquaculture.* 15 (1978) 151–170. [https://doi.org/https://doi.org/10.1016/0044-8486\(78\)90060-1](https://doi.org/https://doi.org/10.1016/0044-8486(78)90060-1).
- [163] A. Jurado, P. Sánchez, J.A. Armesto, R. Guanache, B. Ondiviela, J.A. Juanes, Experimental and Numerical Modelling of an Offshore Aquaculture Cage for Open Ocean Waters, (2018). <https://doi.org/10.1115/OMAE2018-77600>.
- [164] Y.I. Chu, C.M. Wang, J.C. Park, P.F. Lader, Review of cage and containment tank designs for offshore fish farming, *Aquaculture.* 519 (2020) 734928. <https://doi.org/https://doi.org/10.1016/j.aquaculture.2020.734928>.

- [165] P. Klebert, P. Lader, L. Gansel, F. Oppedal, Hydrodynamic interactions on net panel and aquaculture fish cages: A review, *Ocean Eng.* 58 (2013) 260–274. <https://doi.org/https://doi.org/10.1016/j.oceaneng.2012.11.006>.
- [166] Y. Shen, M. Greco, O.M. Faltinsen, I. Nygaard, Numerical and experimental investigations on mooring loads of a marine fish farm in waves and current, *J. Fluids Struct.* 79 (2018) 115–136. <https://doi.org/https://doi.org/10.1016/j.jfluidstructs.2018.02.004>.
- [167] X. Qu, F. Hu, T. Kumazawa, Y. Takeuchi, S. Dong, D. Shiode, T. Tokai, Deformation and drag force of model square fish cages in a uniform flow, *Ocean Eng.* 171 (2019) 619–624. <https://doi.org/https://doi.org/10.1016/j.oceaneng.2018.12.016>.
- [168] H. Cheng, L. Li, K.G. Aarsæther, M.C. Ong, Typical hydrodynamic models for aquaculture nets: A comparative study under pure current conditions, *Aquac. Eng.* 90 (2020) 102070. <https://doi.org/https://doi.org/10.1016/j.aquaeng.2020.102070>.
- [169] T. Kristiansen, O.M. Faltinsen, Modelling of current loads on aquaculture net cages, *J. Fluids Struct.* 34 (2012) 218–235. <https://doi.org/https://doi.org/10.1016/j.jfluidstructs.2012.04.001>.
- [170] T. Kristiansen, O.M. Faltinsen, Experimental and numerical study of an aquaculture net cage with floater in waves and current, *J. Fluids Struct.* 54 (2015) 1–26. <https://doi.org/https://doi.org/10.1016/j.jfluidstructs.2014.08.015>.
- [171] T.-J. Xu, Y.-P. Zhao, G.-H. Dong, Y.-C. Li, F.-K. Gui, Analysis of hydrodynamic behaviors of multiple net cages in combined wave–current flow, *J. Fluids Struct.* 39 (2013) 222–236. <https://doi.org/https://doi.org/10.1016/j.jfluidstructs.2013.02.011>.
- [172] J. V Aarsnes, H. Rudi, G. Løland, 12. Current forces on cage, net deflection, in: *Eng. Offshore Fish Farming*, n.d.: pp. 137–152. <https://doi.org/10.1680/ioceeff.16019.0012>.
- [173] L.C. Gansel, T.A. McClimans, D. Myrhaug, Average Flow Inside and Around Fish Cages With and Without Fouling in a Uniform Flow, *J. Offshore Mech. Arct. Eng.* 134 (2012). <https://doi.org/10.1115/1.4006150>.
- [174] L.C. Gansel, D.R. Plew, P.C. Endresen, A.I. Olsen, E. Misimi, J. Guenther, Ø. Jensen, Drag of Clean and Fouled Net Panels – Measurements and Parameterization of Fouling, *PLoS One.* 10 (2015) e0131051. <https://doi.org/10.1371/journal.pone.0131051>.
- [175] Y.-P. Zhao, C.-W. Bi, G.-H. Dong, F.-K. Gui, Y. Cui, C.-T. Guan, T.-J. Xu, Numerical simulation of the flow around fishing plane nets using the porous media model, *Ocean Eng.* 62 (2013) 25–37. <https://doi.org/https://doi.org/10.1016/j.oceaneng.2013.01.009>.
- [176] C.-W. Bi, Y.-P. Zhao, G.-H. Dong, Y.-N. Zheng, F.-K. Gui, A numerical analysis on the hydrodynamic characteristics of net cages using coupled fluid–structure interaction model, *Aquac. Eng.* 59 (2014) 1–12. <https://doi.org/https://doi.org/10.1016/j.aquaeng.2014.01.002>.
- [177] Ø. Patursson, M.R. Swift, I. Tsukrov, K. Simonsen, K. Baldwin, D.W. Fredriksson, B. Celikkol, Development of a porous media model with application to flow through and around a net panel, *Ocean Eng.* 37 (2010) 314–324. <https://doi.org/https://doi.org/10.1016/j.oceaneng.2009.10.001>.
- [178] C. Balash, B. Colbourne, N. Bose, W. Raman-Nair, Aquaculture Net Drag Force and Added Mass, *Aquac. Eng.* 41 (2009) 14–21. <https://doi.org/https://doi.org/10.1016/j.aquaeng.2009.04.003>.